QUARTERLY PROGRESS REPORT NO. 5

CONTRACT NASW-1035

RESEARCH ON GRAVITATIONAL MASS SENSORS

15 OCTOBER 1965 THROUGH 14 JANUARY 1966

HUGHES RESEARCH LABORATORIES • MALIBU

HUGHES RESEARCH LABORATORIES
Malibu, California

a division of hughes aircraft company

RESEARCH ON GRAVITATIONAL MASS SENSORS

Quarterly Progress Report No. 5
Contract No. NASW-1035
15 October 1965 through 14 January 1966

Robert L. Forward, Principal Investigator
Curtis C. Bell, J. Roger Morris,
J. M. Richardson, and Larry R. Miller,
Contributors

TABLE OF CONTENTS

LIST OF ILLUSTRATIONS

I. INTRODUCTION AND SUMMARY

A. Purpose and Technical Objectives

The ultimate objective of our work on gravitational mass sensors is the development of a small, lightweight, rugged sensor to be used on lunar orbiters to measure the mass distribution of the moon and on deep space probes to measure the mass of the asteroids. The basic concepts, the theoretical limitations, and the possible applications have been investigated and are discussed in Section II of Quarterly Progress Report No. 1.

The purpose of the present research program is

1. To develop and refine experimental techniques for the measurement of gravitational and inertial fields using rotating elastic systems.

2. To develop a more complete understanding of these types of sensors so that accurate predictions of sensor behavior can be made which are based on practical system configurations and measured device sensitivity.

B. Summary of Problem Areas

The major problem area can be summarized in one word — noise. This noise includes background clutter due to external forces and masses other than the one under investigation, external electrical noise and mechanical vibrations, and internal thermal and electronic noise in the sensor and amplifiers. The force of gravitational attraction is very weak, even for large masses, and every effort must be made in sensor design and operation to develop and utilize discrimination techniques that will allow the weak gravitational signal to be picked out from the background clutter and noise.

The problems of background clutter are nearly independent of the particular sensor design. It is felt that the techniques discussed in Section II-D-2 of Quarterly Progress Report No. 1, Background Rejection, will suffice for elimination of this source of noise.

The problems of externally and internally generated electrical and mechanical noise have been overcome in previous work on non-rotating gravitational sensors and the experience gained during this work will aid in the investigation of the very similar problems in rotating sensors. It is expected that each sensor design will have its own

versions of these problems and that a major portion of the experimental work will be spent in locating and eliminating or discriminating against these sources of extraneous noise.

One minor problem area which will require special attention in the theoretical portion of the program is the instability and cross-coupling effects that are common to mechanically rotated systems. Typical examples are given in the Appendix of Quarterly Progress Report No. 1 and Section III of this report. These problems can be avoided by proper choice of sensor configuration and sensor operation based on a thorough theoretical analysis and preliminary experimental studies of each proposed design before extensive experimental work is done.

C. Summary of General Approach

The program has started with parallel efforts consisting of detailed theoretical study and preliminary experimental work. The various possible sensor configurations are being investigated theoretically to determine their suitability as mass sensors under the assumed operating conditions. Various combinations of promising sensor designs and sensor support and drive mechanisms are being constructed and operated to verify qualitatively the sensor characteristics, develop signal read-out techniques, and search for unexpected sources of instabilities and noise. No attempt will be made to look for gravitational interactions at this stage.

After the preliminary work, one of the sensor configurations will be chosen as the basis for a feasibility model, and a carefully designed version will be constructed. The remainder of the program will be expended in studying the feasibility model both experimentally and theoretically, locating and eliminating the sources of extraneous noise, and determining the sensitivity to gravitational fields. The program objective is a sensor that will detect the presence of a small, nearby moving mass through gravitational interactions.

D. Summary of Work to Date

This work began when the completed contract was received on 26 October 1964. The original study by R. L. Forward on the gravitational mass sensor was analyzed by C. C. Bell in a more general manner. (See Appendix of Quarterly Progress Report No. 1.) This analysis indicates that radially vibrating sensor structures generally are incapable of measuring the gravitational force gradient because the sensor will fly apart at the necessary rotation speeds.

The most promising form of gravitational mass sensor has been found to be a cruciform shaped spring-mass system. A number of different cruciform sensor heads have been designed and studied experimentally. They all have demonstrated a basic structural stability under high rotation speed. A continuing theoretical study of the transversely vibrating cruciform sensor structure has been under way. The model used for the analysis consists of a central mass, four equal sensing masses on transversely vibrating arms, and a sensed mass. The analysis is quite complicated because of the multiplicity of masses and springs, the nonuniform character of the gravitational field, and the requirement that the restoring forces in the sensor include the centrifugal force as well as the spring constant of the arms. The results of these analyses indicate that there is a particular mode of vibration of the sensor — the tuning fork mode (see Fig. 16 in this report) — whose frequency is different from that of other modes, responds to the presence of a gravitational force gradient field when rotated at half of its vibrational frequency, and yet does not respond to inertial forces.

The readout of the very small (10^{-10} in.) vibrations in the sensor arms is accomplished by the use of piezoelectric strain transducers attached to the sensor arms at the point of maximum strain. These transducers have a voltage-strain characteristic of 10^5 V/unit strain and have been used in previous work to measure motions down to 10^{-13} in. The voltage output expected of such a sensor due to the gravitational force gradient of a mass M at a distance R is

$$V = \frac{3GM\,Q\,3cr}{2R^3\,(2\omega)^2L^2}\,\sigma \sin 2\omega t \approx \frac{3GM\,\tau\,3cr}{2R^3(2\omega)L^2}\,\sigma \sin 2\omega t \qquad (1)$$

where

$Q \equiv$ quality factor of the sensor resonance

$GM/R^3 \equiv$ gravitational gradient

$\omega \equiv$ angular frequency of rotation of the sensor

$\tau \equiv$ integration time $\approx \frac{Q}{2\omega}$

$r \equiv$ radial distance of sensor end mass from center of sensor rotation

$L \equiv$ length of sensor arm

$c \equiv$ half thickness of sensor arm

$\sigma \equiv$ transducer factor of strain transducer ($\sim 10^5$ V/in./in.).

If we assume a gravitational gradient caused by the earth (1.5×10^{-6} sec^{-2}), the voltage output from the present monolithic sensors with a Q of 100 and a resonant frequency of 115 Hz is greater than 4 μV. These voltages are easily measured with standard laboratory equipment.

Although our primary goal under this contract is to find methods of rotating the gravitational mass sensor structures without introducing large amounts of noise into the gravity gradient sensing mode, one objective of our work is to learn enough about these structures to be able to predict their response to gravitational gradient fields. The theoretical portion of this work is largely completed, and was reported in the Appendix of Quarterly Progress Report No. 3. In order to verify these equations experimentally and to develop a test system for calibrating the gravitational gradient response of the various mass sensors which we will be using, we have constructed a generator of ac gravitational gradient fields and have measured the response of one of our sensors to these fields (see Section II-E of this report.) The generator consists of two 1-kg masses rotated at 44 rps (2640 rpm) on the air bearing supported motor originally designed to rotate the sensor structures. The detector is one of the adjustable sensors which resonates at 88 Hz. The nongravitational coupling between the generator and detector is so low that ac gravitational gradient fields as small as 1/20 of the earth's gradient can be seen. These experiments demonstrate that the gravitational mass sensor structures and our present electronic subsystems are more than adequate for the purpose of detecting gravitational force gradients as small as 10^{-7} sec^{-2}, our sole remaining problem for this research phase of our work on gravitational mass sensors is a continued effort to reduce the noise leaking into the sensor mode under rotating conditions to the point where the signals from the earth's gravitational gradient can be seen.

One of the problems which has arisen in our study of cruciform sensors is that of maintaining adequate frequency separation between the gravitational gradient sensing mode of the sensor and the other possible modes of vibration of the sensor and the sensor mounting structure. If the sensor head is held too firmly by the sensor mount, the sensor vibrational modes all converge to the same frequency. If the sensor is held too loosely, the sensor mount cannot resist the centrifugal force when the sensor is rotated. When the sensor is rotating, the modes tend to shift in frequency in a complicated, but predictable, manner. This often brings the gradient sensing mode frequency close to one of the other mode frequencies, making it difficult to utilize frequency filtering techniques to separate out the gravitational gradient signals. However, the results of the combined theoretical and experimental program on the behavior of the sensor modes under rotation indicates that by proper design of the sensor and sensor mount, it is possible to operate the sensor at the desired rotation speed of one-half of the gradient sensing mode frequency and still maintain adequate frequency separation.

Since the sensors must be rotated in order to work, the major problem being studied is that of bearing noise. A number of different bearings have been fabricated for our purposes and their noise characteristics investigated.

A ball bearing mount using gyro bearings and a carefully balanced sensor was constructed first. (See Section III of Quarterly Progress Report No. 1.) This type of bearing proved, as expected, to be much too noisy for use with these sensors.

An air bearing support and drive was then constructed by the Hughes Aerospace Group. The structure consists of a table supported both vertically and horizontally by an air bearing formed between a rotor tube and a channeled stator. The rotor tube also has a magnetic hysteresis ring which is driven by a synchronous motor stator constructed around the outside (see Section II-C of Quarterly Progress Report No. 2). The sensor chamber is then mounted on top of the rotor table and the voltages from the sensor are removed through the slip rings on the top.

A single-axis magnetic bearing support and drive was fabricated by the University of Virginia (see Section II-B of Quarterly Progress Report No. 3). In general, the unit performs well and is quite satisfactory for this program. The levitation circuits are slightly tricky in adjustment, but have proved to be capable of stably levitating the 6 lb mass of the sensor chamber and the iron pole cap. The compliance of the magnetic "spring" is very low so that there is good vibration isolation at the sensor frequency. When the servo loop is properly adjusted, the vertical stability of the support is good, except for a long term drift which requires that the servo gain be adjusted periodically. The pancake motor drive works quite well, although the available torque is necessarily limited by the relatively large air gaps which result from the levitation requirements.

Noise tests were conducted on these bearings using a sensor on a torsion wire mount inside a vacuum chamber. Readout was accomplished by means of slip rings running directly into a General Radio tuned preamplifier having an equivalent input noise of 0.050 μV. The first tests were undertaken to discover the sources of noise in the bearings under nonrotating operation. When the sensor chamber was suspended from a rubber band, the noise output was essentially flat with a amplitude of about 0.1 μV. When the sensor was sitting on the air bearing with no air flowing through the bearing, the noise output was essentially flat with an amplitude of about 0.2 μV. The increase in noise output resulted from the vibrations in the workbench. When the air pressure was turned on, levitating the sensor, the noise increased considerably. The background level was then 0.6 μV with a

peak at the translational mode (220 Hz) of 10 μV, and a peak at the gradient sensing mode (170 Hz) of 1.5 μV. Several air bearing rotors with various gaps were tested, with the result that the noise seemed to be linearly proportional to the amount of air flow. When the iron pole cap was attached to the sensor chamber and suspended in the magnetic bearing, the background noise level was about 0.15 μV.

Bearing noise tests were then made under dynamic conditions. The first tests were made by bringing the sensor up to speed, turning the drive off, and measuring the noise output as the sensor coasted down. It was found, in general, that under dynamic as well as static tests, the air bearing is 14 dB or more noisier than the magnetic bearing. This excess noise seems to result from the rush of air through the bearing and there is no obvious way to eliminate the problem. These tests indicated that for our purposes a magnetic support generally is superior to the air bearing support.

On the basis of these tests it was decided to utilize a magnetic bearing in the feasibility model. A three-axis magnetic bearing and drive was ordered from the Cambridge Thermionic Corp. (CAMBION) in Cambridge, Massachusetts. This unit will have a smaller size and weight than the present bearing, it will have tighter tolerances on drift, and it can be oriented in any direction. The original delivery date for this bearing was 15 November 1965. This date has slipped three months, and CAMBION now anticipates delivery by 15 February 1966. The contract work completion date was also 15 February 1966. Since no time would remain for a study of the performance of the three-axis bearing, it was necessary to obtain a two month extension of the contract. The extrapolated expenditure curve indicates that this can be done within the authorized contract cost limit.

While the three-axis magnetic bearing is being fabricated, the single-axis bearing was reworked to improve its performance and an external vacuum chamber added to reduce air drag effects on the rotating sensor chamber. This unit was used for an extended series of vibrational mode tests, sensor mount studies, and bearing noise tests.

When noise tests were made with the magnetic support motor drive on, two additional noise sources resulting from the drive fields were found. One was a general noise level increase due to hash and hum in the drive amplifiers. This caused about 3 μV of noise and was seen only when the drive amplifiers were turned on but the sensor was not yet rotating. This noise will be eliminated by filtering the output of the drive amplifiers. The second was a torquing noise resulting from the interaction of the rotating drive field and the remnant magnetic poles in the hysteresis plate. This noise is a direct function of the drive power and, for synchronous operation with large drive levels, can be many millivolts. However, if the drive is lowered to a level just sufficient to maintain synchronous rotation, or if the phase locked asynchronous drive (see Section II-A of this report) is used, the noise level drops to the level seen under free rotation conditions.

A set of noise measurements were taken on a sensor mounted on a 0.020 in. diameter torsion wire inside an evacuated sensor chamber. Although this sensor system was the best available at the time, it still had a vibration sensitive translational mode within a few hertz of the gradient sensing mode. Three tests were run; the first used regular slip ring brushes while the sensor chamber was run in air. The second test was the same as the first except that the external vacuum chamber was added and evacuated in order to cut down windage noise. The data show that the difference between air and vacuum for this configuration was very slight, indicating that windage is not yet a problem. However, the slip ring brushes were found to be responsible for the large noise peaks (200 mV) at the rotational speeds corresponding to the translational mode and the gradient sensing mode. In the third test, the standard slip ring brushes were replaced with special fine copper wire brushes with low mass and low mechanical coupling. The data taken with the light slip ring brush had a maximum noise peak of about 8 mV at 108 Hz when the sensor was rotating at the desired operating speed of 3240 rpm (54 rps).

Since slip ring wobble seemed to be a major source of noise, a telemetry unit was constructed. It has been up to operating speed with the sensor suspended from it. Noise tests on the telemetry amplifier and transmitter indicate that pickup and vibration from the bearing fields and drive fields are negligible.

Because of the mode separation problem encountered using a double-ended torsion wire mount for the sensor, a single-ended sensor mount was investigated. This consists of a very thin, low frequency mount which is operated far above its translational resonance point in a manner similar to an ultracentrifuge. The preliminary tests with a fine wire support gave good results. The various vibrational modes were sufficiently separated that they could be easily resolved, and the maximum output at the gradient sensing mode frequency (117 Hz) when the sensor was rotating at the desired rotational speed (58.5 rps) was 500 μV. This is an improvement of an order of magnitude over the results obtained using the double ended mount. The major portion of this noise appeared to be caused by electrical and magnetic interactions and vertical vibrations of the support transmitted to the sensor head through the suspension wire.

The test set up was modified by enclosing the sensor head in a mu metal case and suspending it from a rubber band rather than the torsion wire. The signals from two pairs of opposed strain transducers were then fed into the differential input of a lock-in amplifier which was phase locked through a photoelectric pickup to paint marks on the rotating sensor. Two peaks were seen: one, at 62 rps rotation, was the response of the translational mode at 124 Hz; the other, at 58.5 rps, was the response of the tuning form or gravitational gradient sensing mode at 117 Hz and had an amplitude of about 60 μV.

Data were then taken at various vacuum levels between 0.022 Torr and 0.160 Torr. The data indicate an approximately linear relationship between noise level and pressure throughout the range measured. Actual noise levels measured ran from 60 μV per transducer at 0.022 Torr pressure to 300 μV per transducer at 0.160 Torr pressure. The gravity gradient signal expected in the laboratory is 4 μV or approximately 6% of the lowest noise figure read.

We were unable to reduce the pressure of the system below 0.022 Torr with the equipment then available, but we are currently adding a diffusion pump to our vacuum system which should allow the pressure to be reduced an additional order of magnitude. Although the noise level test data indicate significant noise-pressure dependence, it must be remembered that the sensor head is rotating in the external vacuum chamber without the usual co-rotating sensor vacuum chamber, and is, in effect, "windmilling" the remaining air molecules about in the chamber. A sensor vacuum chamber is being manufactured with adequate space for the ultracentrifuge suspension, which will eliminate the "windmilling" and should reduce the remaining acoustic noise to minimal levels.

The analysis of the vibrational mode behavior of cruciform gravitational mass sensors which was included in Quarterly Progress Report No. 4 was extended to include the sensor mounting structure. The solutions obtained for the sensor mode frequencies agree well with the measured mode frequencies. A paper covering both the theoretical and experimental aspects of the vibrational mode behavior was submitted to the AIAA/JACC Guidance and Control Conference in Seattle, Washington, on 15 - 17 August 1965, and is included as the Appendix to this report.

A shortened version of Quarterly Progress Report No. 1 was submitted to the annual essay contest of the Gravity Research Foundation, New Boston, New Hampshire, as an essay entitled "Rotating Gravitational Sensors" by R. L. Forward, C. C. Bell, and J. R. Morris. The essay received the fourth award.

A paper, "Mass Detection by Means of Measuring Gravity Gradients," by C. C. Bell, R. L. Forward, and J. R. Morris was prepared for the 2nd Annual AIAA Meeting and was given by Curtis Bell on 26 July 1965 in San Francisco.

II. EXPERIMENTAL PROGRAM

A. Asynchronous Drive

One requirement of our mass sensing study is that the sensor be rotated at one half the tuning fork resonant frequency. Furthermore, the instantaneous position (phase) of the sensor must be known for processing the data. The synchronous drive built into the single-axis magnetic suspension has not been completely satisfactory for our purposes. First, the motor drive frequency is twice the synchronous speed — exactly the sensor output frequency. Thus it is not possible to use frequency discrimination techniques to eliminate electrical pickup from the drive. In addition, there is no control over the oscillation of the rotor between the synchronously rotating poles, other than by varying the drive intensity.

In order to overcome these difficulties, an asynchronous drive system invented by Larry Miller has been constructed and tested. The important features of this system are

1. Any frequency higher than the sensor frequency may be used to drive the rotor.

2. The rotor speed may be synchronized with an external frequency.

3. Well damped phase lock is achieved.

The theory of operation can be seen by reference to the block diagram in Fig. 1.

1. A photoelectric pickoff produces one spike per rotor revolution.

2. This spike operates a gate which allows a reference frequency sine wave to be scrutinized.

3. When the spike and reference frequency are synchronous, the voltage level of the reference will be the same each time the gate is opened. This level, and its derivative (for damping), are used to control a variable gain amplifier through which the drive frequency passes.

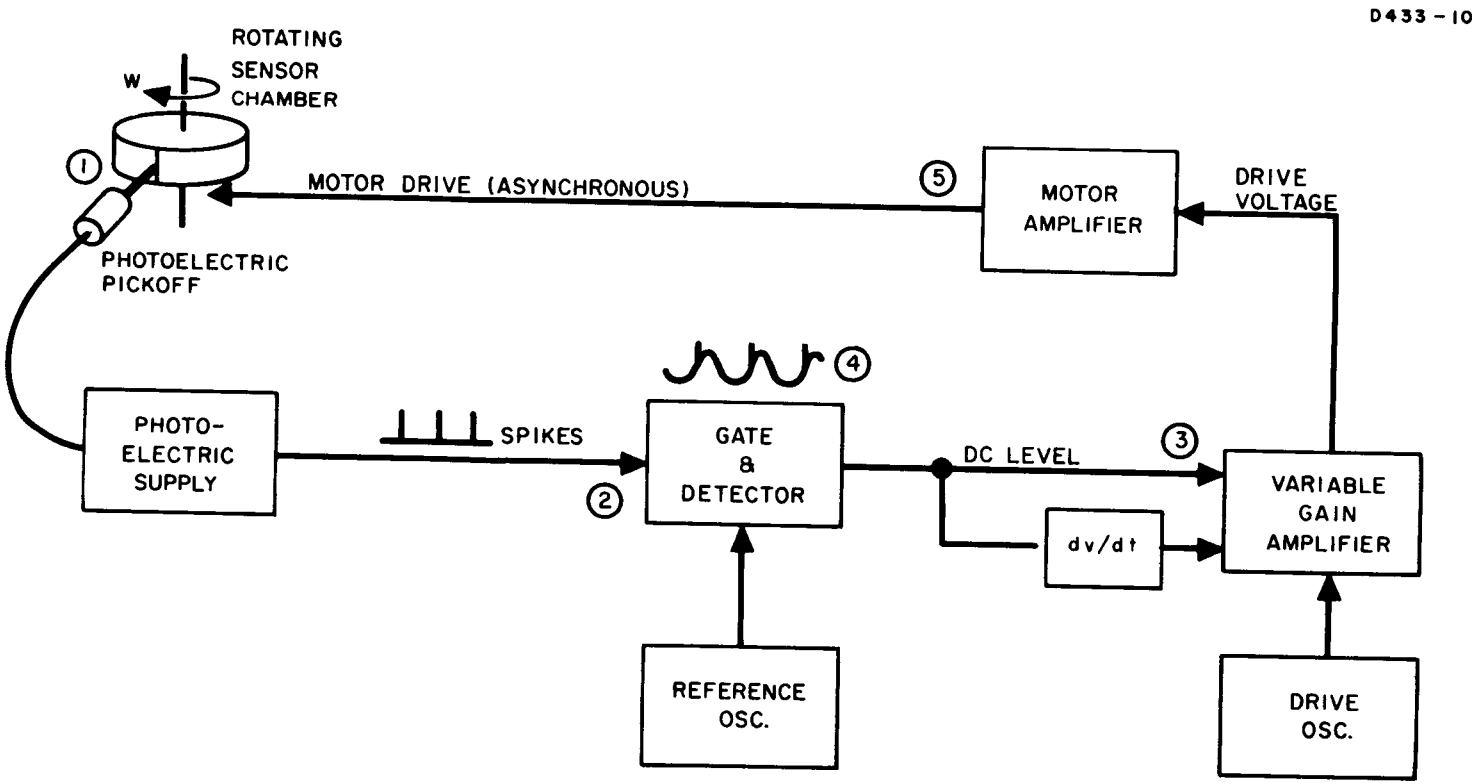

Fig. 1. Block diagram of asynchronous drive.

4. If the rotor rotation rate falls behind the reference frequency, the spike position moves down the reference sine wave, sampling a lower level. The lower level increases the drive frequency amplification, causing the rotor to speed up.

5. The rotor is thus forced to maintain a fixed position relative to the reference phase, and the drive frequency may be any frequency above the reference frequency.

Two of these drive units have been constructed, one for use on the magnetic bearing and the other for the motor on the air bearing. They are slightly more complicated to set up and operate than the synchronous drive, but work well. The schematic for the electronics is shown in Fig. 2. The circuit is believed to be novel, and a patent disclosure has been submitted to NASA through the Hughes patent office.

B. Telemetering System

The necessity for a frictionless and vibrationless method of routing the signals from the sensor to the processing electronics, and a description of an amplifier-transmitter for this purpose, were discussed in Quarterly Progress Report No. 3. Several problems encountered in testing that system have been eliminated in the revised version now in use. A physical drawing of the new design is shown in Fig. 3 and a schematic in Fig. 4.

The two major difficulties with the old design were mechanical instability and low battery capacity. These have both been solved by placing four batteries and the electronics inside the rotor. The system is now quite stable at rotation speeds over 60 rps and has a battery life of over 40 hours.

1. Differential Input

The sensor must hang several inches below the rotor on a rubber band or other compliant support. The wires which lead from the sensor to the electronics in the rotor must be very thin, flexible, and light. This precludes using shielded wires. Because these wires rotate within a strong magnetic field, clutter voltages are generated at the rotation frequency and its harmonics.

Several methods of reducing this clutter are available, one of which is a differential input. The gauges are connected as shown in Fig. 5. This connection gives an output which is maximum for the "tuning fork" mode when A and B are out of phase. All common mode signals from either sensor or lead pickup are cancelled.

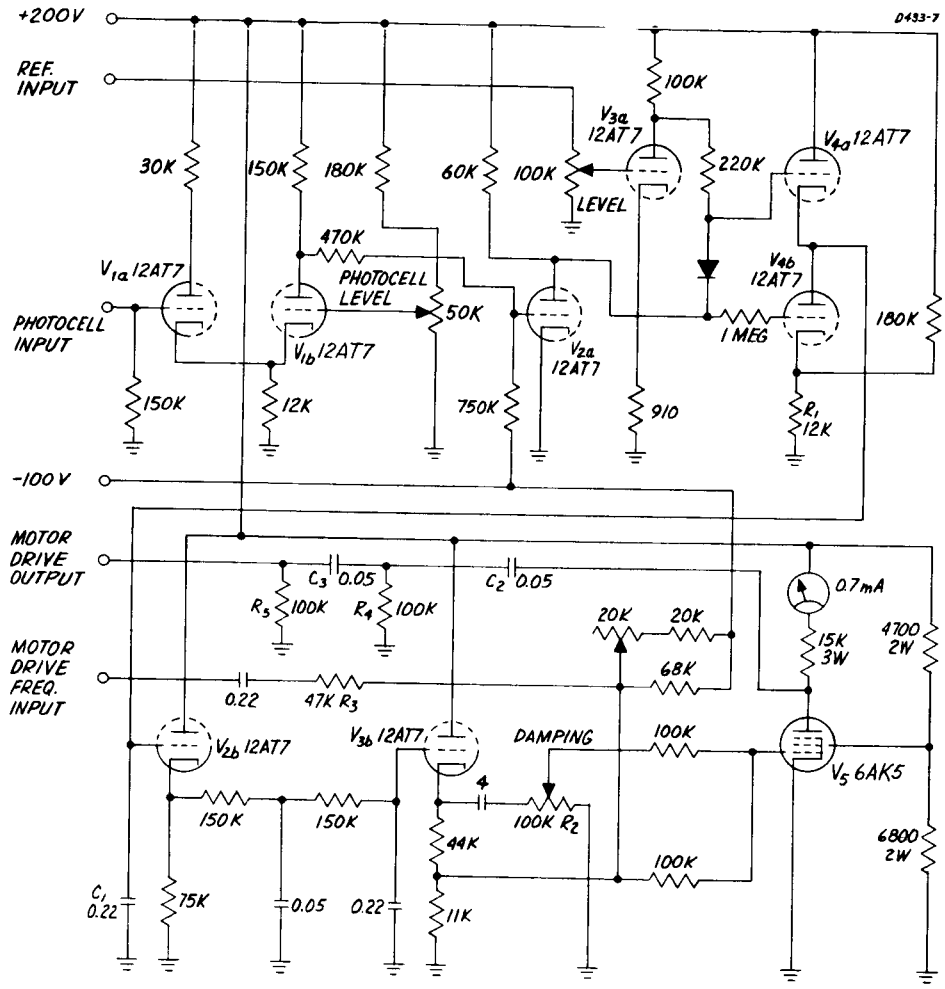

Fig. 2. Schematic of asynchronous drive.

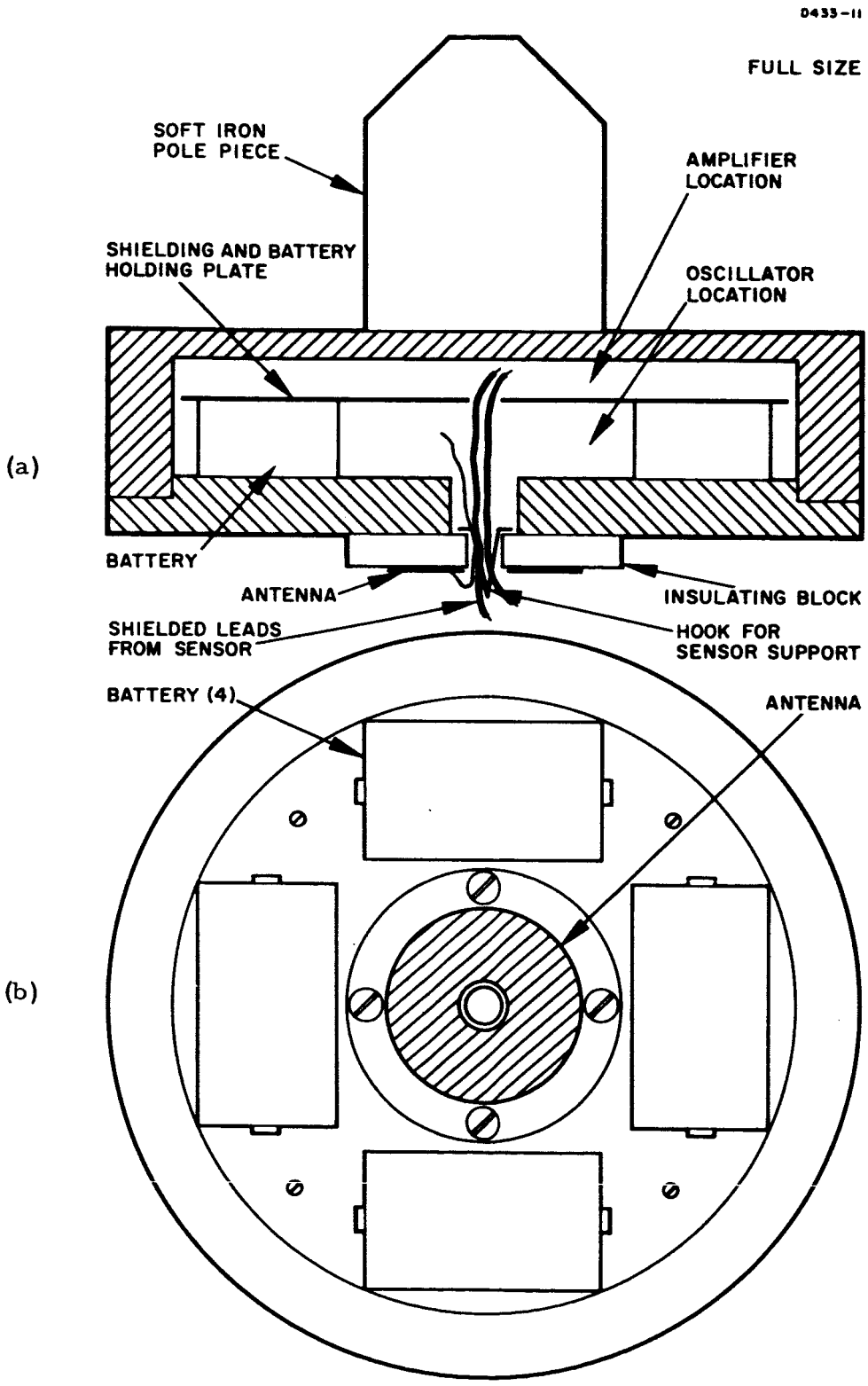

Fig. 3. Telemetering system. (a) Side view. (b) Bottom view.

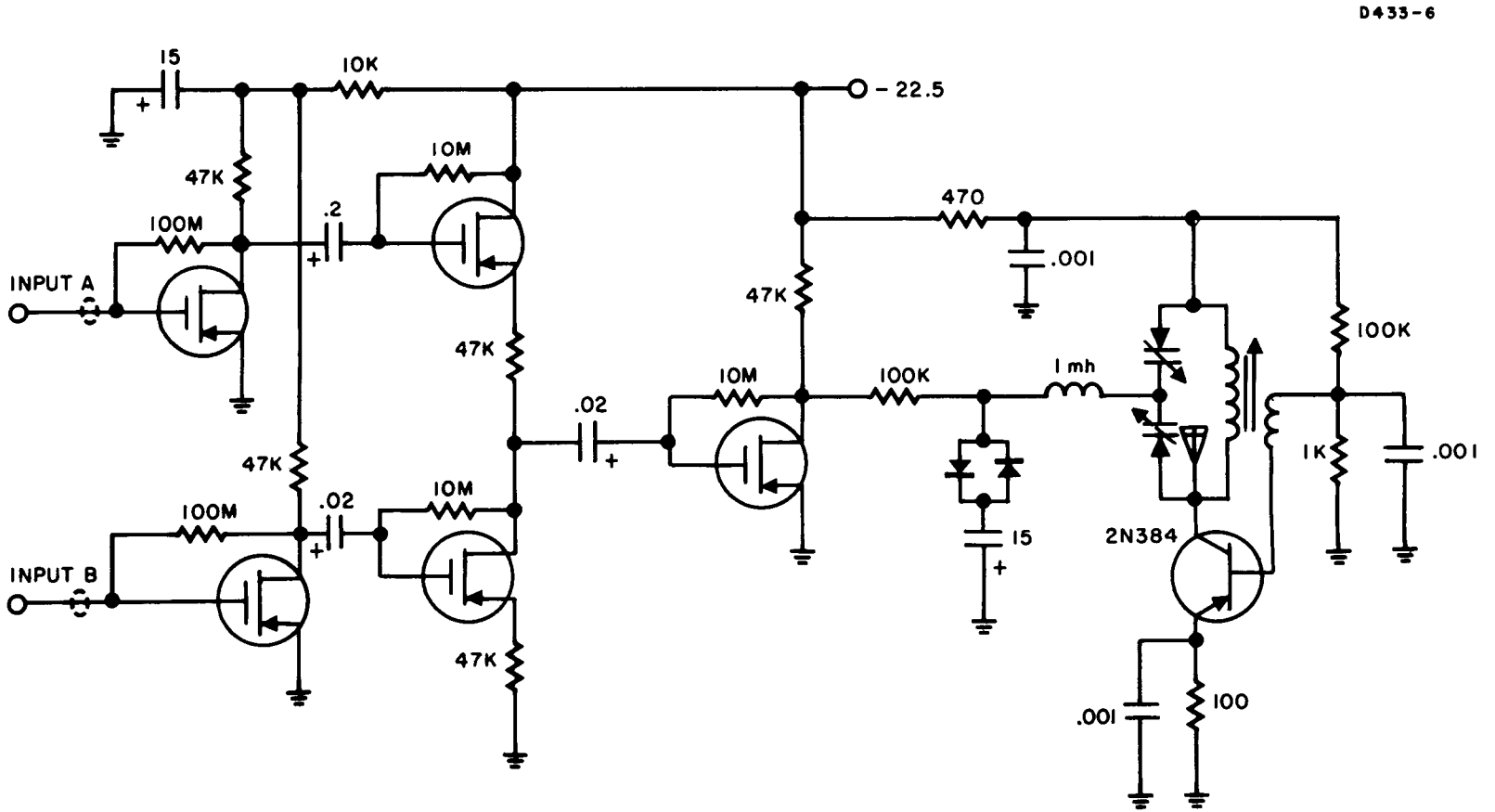

1. ALL CAPACITORS IN uF
2. ALL RESISTORS 1/8 W, 5%
3. ALL MOSFETS 2N3608
4. VARICAPS PC 115
5. COIL MILLER 40A226CB1, 1.50 - 2.75 uh
6. CARRIER FREQ. 36 MHz

Fig. 4. Differential amplifier and FM transmitter.

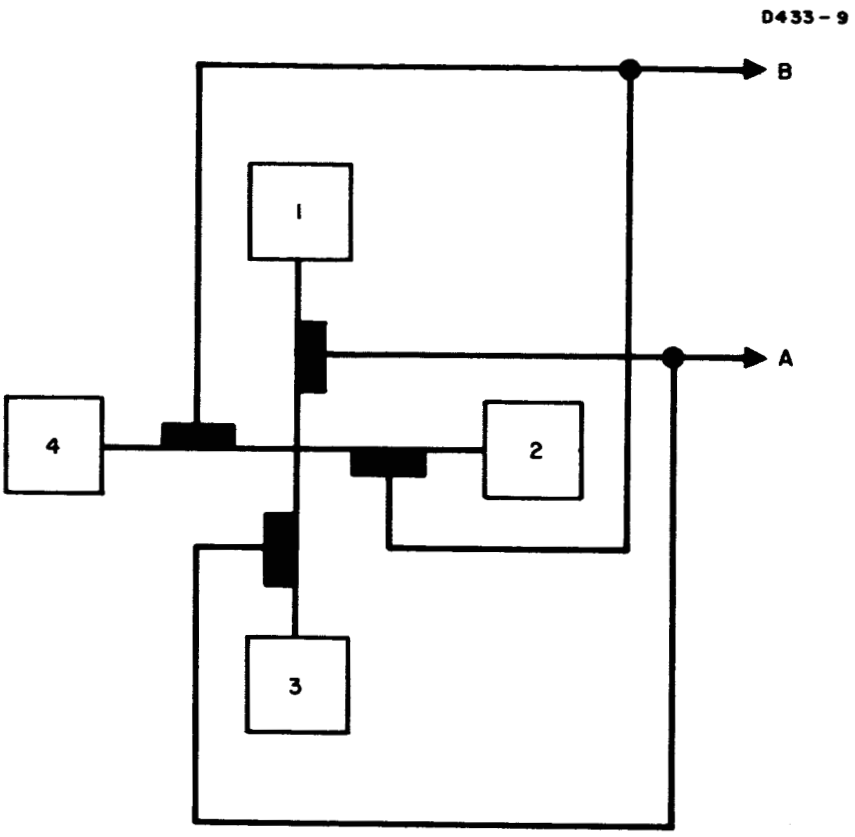

Fig. 5. Gauge connections.

2. Performance

Each input has a 10 MΩ impedance which is 20 times the impedance of two parallel gauges.

The gain from either input through the entire system to the receiver output is 75. The common mode gain is 3.2 giving a common mode rejection ratio of 23.5.

The noise at 100 Hz in a 5% band for the system with sensor connected and rotor suspended on the magnetic bearing and in vacuum is 200 μV, or 2.7 μV referred to the input.

All data are taken with a Hallicrafters Mode SX62B receiver at full gain and a 1000:1 attenuator cable from its output.

The transmission frequency is 37 MHz.

C. Sensor Design Studies

The analytical work reported in Quarterly Progress Report No. 4 (Section III-B) provided a theoretical basis for the operation of the sensor, the results of which are in close agreement with data taken on actual sensor-torsion bar combinations. Based on this theory, it was decided that the performance of the sensor could be improved in the following ways:

- To improve mode separation, a smaller ratio of central mass of the sensor to the outer masses is required
- To minimize the effect of centrifugal force on the resonance curves, the distance from the center of rotation of the sensor to the bending point in the arm should be a minimum compared with the sensor effective radius (see eq. (57), Section III-B, Quarterly Progress Report No. 4).
- To maximize the sensitivity to the gravity gradient field, the effective sensor radius should be maximized.

Based on the above points, a new sensor was designed as illustrated in Fig. 6.

This new sensor was designed to have a maximum end mass to center mass ratio, central bending of the arms, and a large effective radius to help optimize output.

M4572

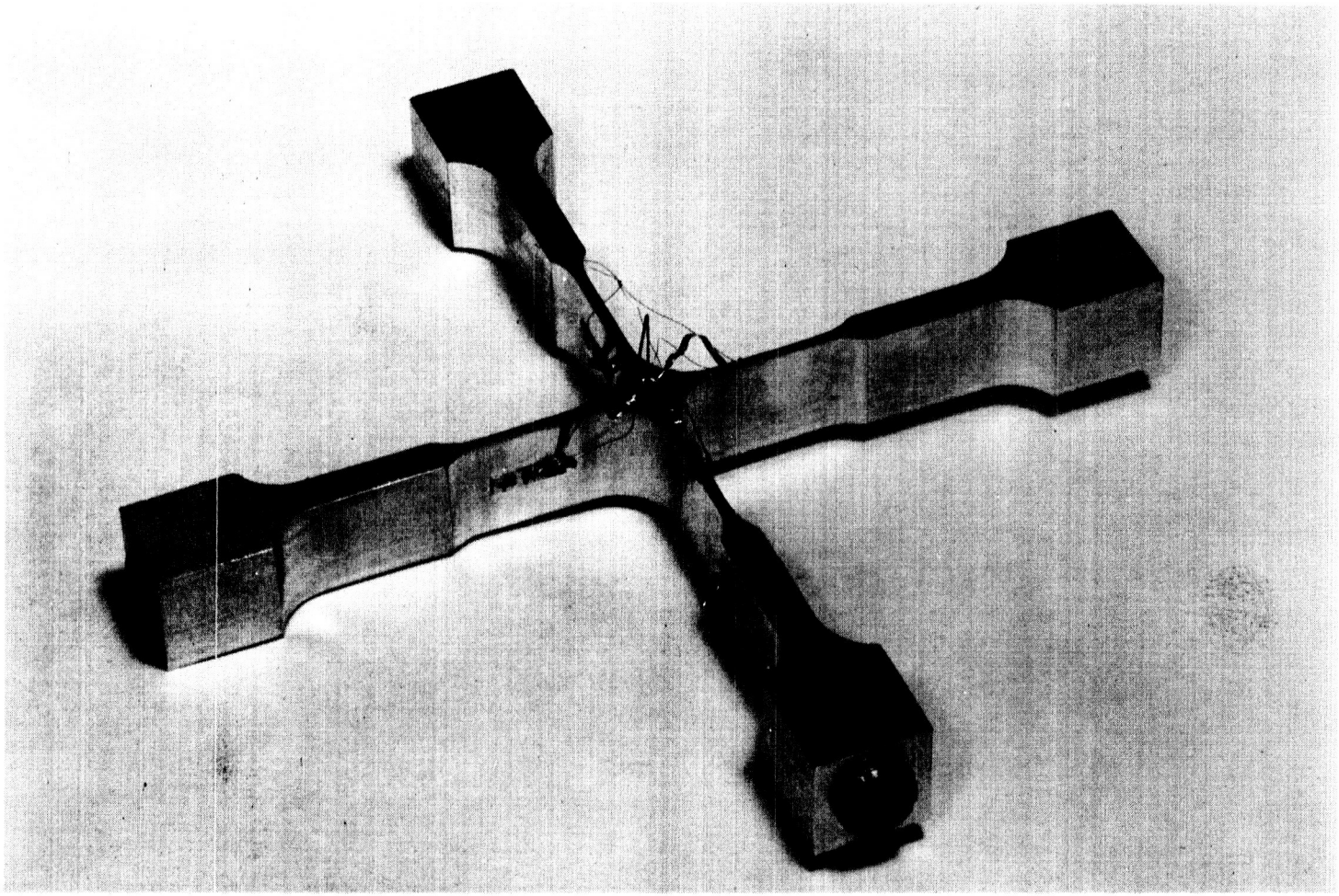

Fig. 6. Seven inch diameter cruciform sensor.

In addition, by including an adjustable brass slug in each end mass, it is possible to adjust the effective radius of each arm in order to match the translational modes of the sensor in both axes.

This sensor has been assembled and is currently being tested for mode response and noise sensitivity.

D. Noise Tests on Rotating Sensors

Because of the mode separation problem which existed when double ended tension wire mounts for the sensor were used, a thin single ended sensor mount was investigated. This mount consisted of a thin (0.020 in. diameter by 6 in. long) wire between the sensor and the magnetic suspension. The mount had a low translational natural frequency and was operated far above its translational resonance point in a manner similar to an ultracentrifuge.

Preliminary tests on this mount gave good results. The various vibrational modes were sufficiently separated that they could be easily resolved, and the maximum output at the gradient sensing mode frequency (117 Hz) when the sensor was rotating at the desired rotational speed 58.5 rps) was 500 μV. This is an improvement of an order of magnitude over the best noise level observed on sensors with double ended mounts, as reported in Quarterly Progress Report No. 4 (p. 22). A large portion of this noise appeared to be a result of electrical and magnetic interactions and vertical vibrations of the support transmitted to the sensor head through the suspension wire. The test setup was then modified by suspending the sensor head from a rubber band rather than from a wire (see Fig. 7).

Signals from opposing pairs of strain gauges in parallel were brought through the fine wire slip rings and fed into the differential input of the Princeton Applied Research HR-8 Lock-In Amplifier (see Fig. 8). While the sensor was rotating its output was phase-locked to its rotation position by means of a photoelectric pickoff observing the sensor's position (see Fig. 9).

The opposing sets of strain transducers were paralleled so that the symmetrical portion of the sensor output in the translational mode would be rejected. In this mode, signals from opposing transducers would be out of phase; if they were paralleled, they could cancel each other. Similarly, the paralleled signals from transducers A and C and transducers B and D were handled differentially in order to reject the symmetrical portion of the sensor in the torsional mode and to reject symmetrical pickup in both channels.

M4612

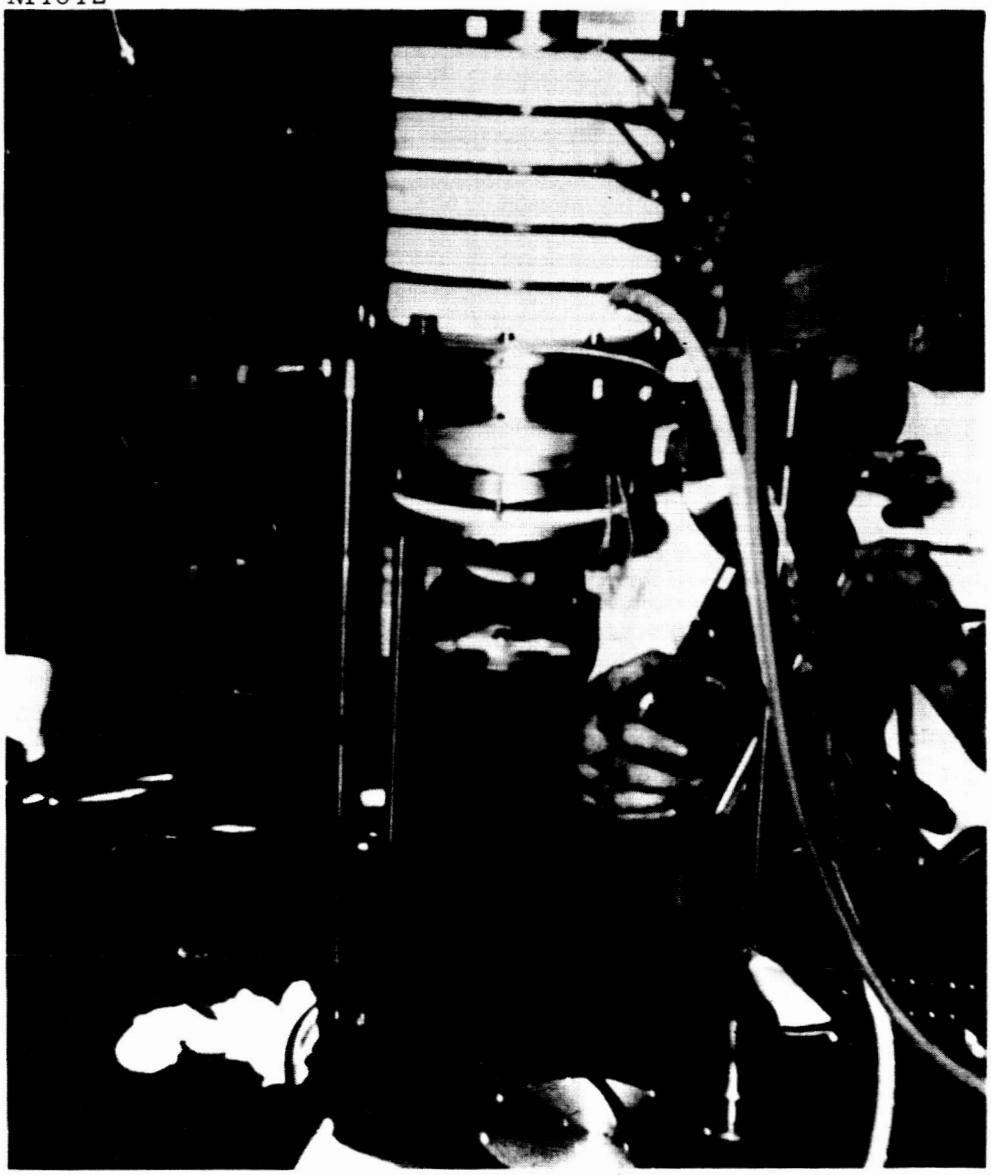

Fig. 7. Sensor rotating on rubber band mounting (without vacuum chamber).

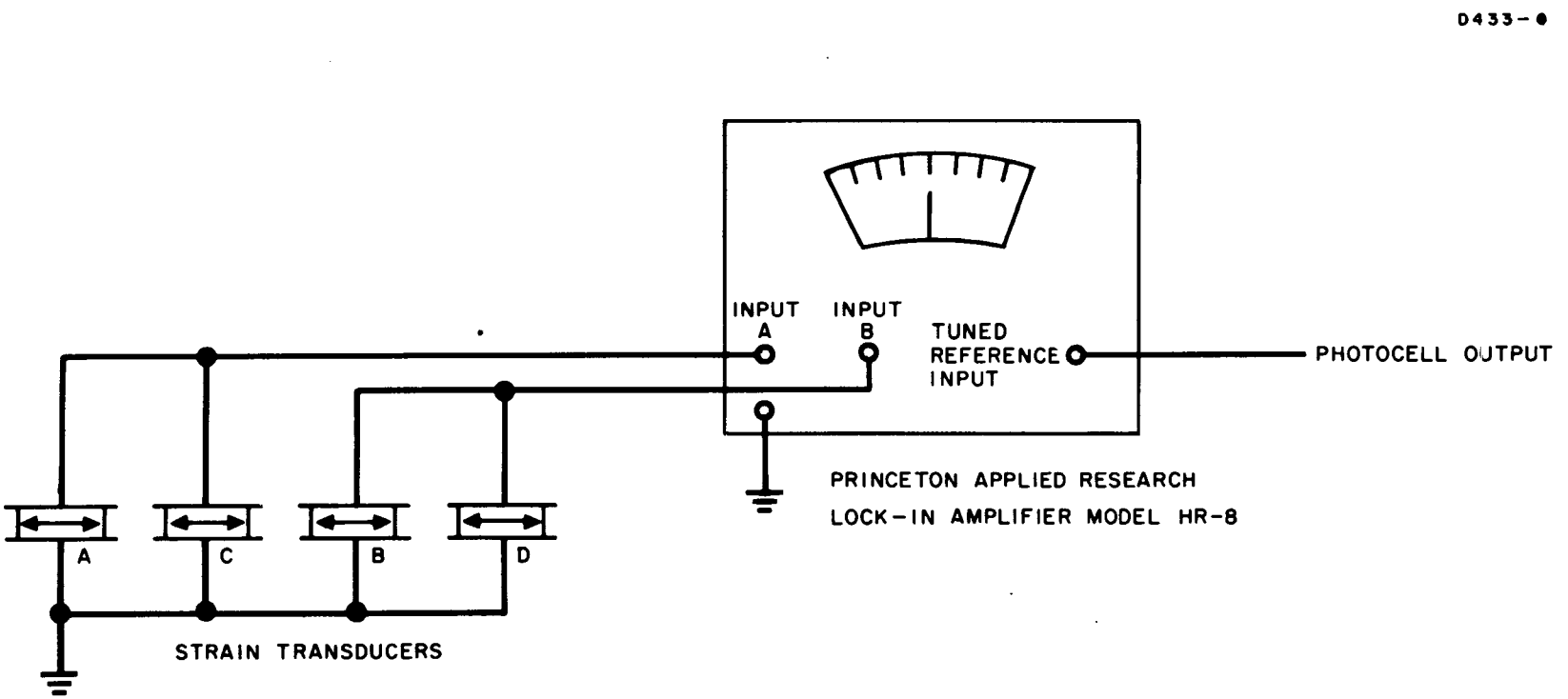

Fig. 8. Electronic block diagram.

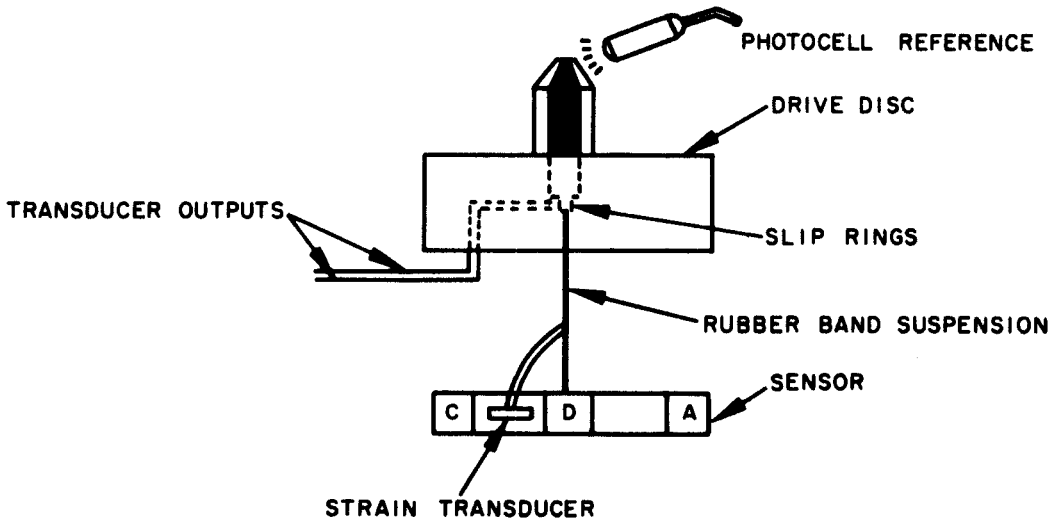

Fig. 9. Rubber band suspension.

Data were taken by running the sensor rotation frequency higher than one half of the translational mode resonant frequency; the drive power was then shut off, and the sensor was allowed to coast down while the output of the sensor was matched against the reference signal generated by the photoelectric pickoff. The resulting noise output data are shown in Fig. 10.

Two peaks can be seen. The peak at 62 rps rotation speed is the response of the translational mode at 124 Hz. The peak at 58.5 rps is the response of the tuning fork or gravitational gradient sensing mode at 117 Hz, and has an amplitude of 60 μV per transducer. The gravity gradient signal expected in the laboratory is 4 μV or approximately 7% of this figure.

The sensor was then driven synchronously with minimum drive power, and the rotation speed was adjusted for peak output in the gravity gradient sensing mode. The vacuum system was then shut off, and the pressure was allowed to rise slowly from 0.022 Torr to 0.16 Torr. Noise data were taken at various points in this range. These data are reproduced in Fig. 11. This graph shows an approximately linear relationship between noise level and vacuum level in the vacuum level range examined. We were unable to reduce the pressure level of the system below 0.022 Torr with the equipment available, but we are currently incorporating a revised vacuum system which should improve our vacuum capability by one to two orders of magnitude. Although the noise level test data indicated significant noise-pressure dependence, it must be remembered that the sensor head is rotating in the external vacuum chamber without the usual co-rotating sensor vacuum chamber and is in effect "windmilling" the remaining air molecules about in the chamber. A sensor vacuum chamber is being manufactured with adequate space for the ultracentrifuge suspension, which will eliminate the "windmilling" and should reduce the remaining acoustic noise to minimal levels.

E. Sensor Calibration Using AC Gravitational Gradient Fields

Although our primary goal is to find methods of rotating the gravitational mass sensor structures without introducing large amounts of noise into the gravity gradient sensing mode, one objective of our work is to learn enough about these structures that we can predict their response to the gravitational gradient field of a mass. The theoretical portion of this work is largely complete and was reported in the paper "Mass Detection by Means of Measuring Gravity Gradients," by Curtis C. Bell, Robert L. Forward, and J. Roger Morris, which was presented at the AIAA Second Annual Meeting in San Francisco on 26 July 1965, and was included as the Appendix in Quarterly Progress Report No. 3. In order to experimentally verify the theoretical equations and to develop a test system for calibrating the gravitational gradient response of the various mass sensors which we will be using, we have constructed a generator of ac gravitational gradient fields and have measured the response of one of our sensors to these fields.

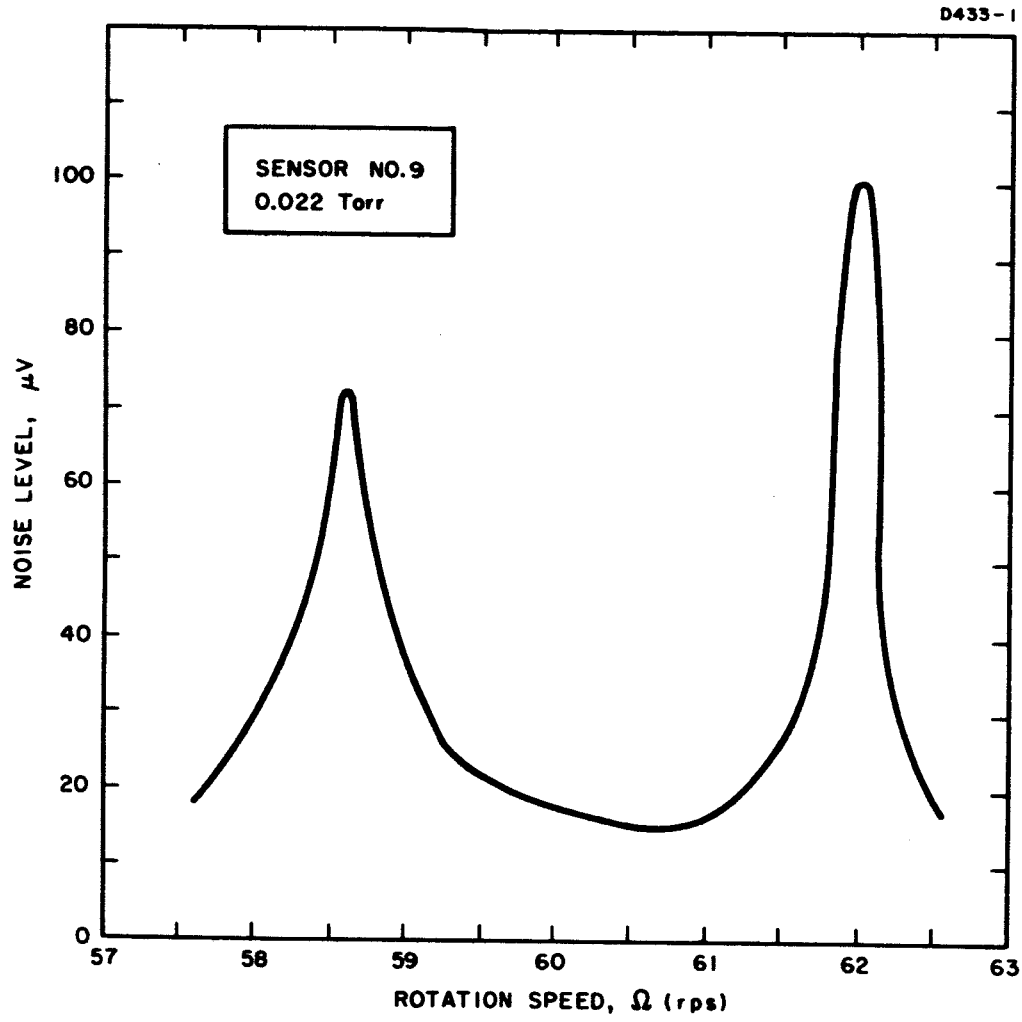

Fig. 10. Noise tests on rubber band suspension.

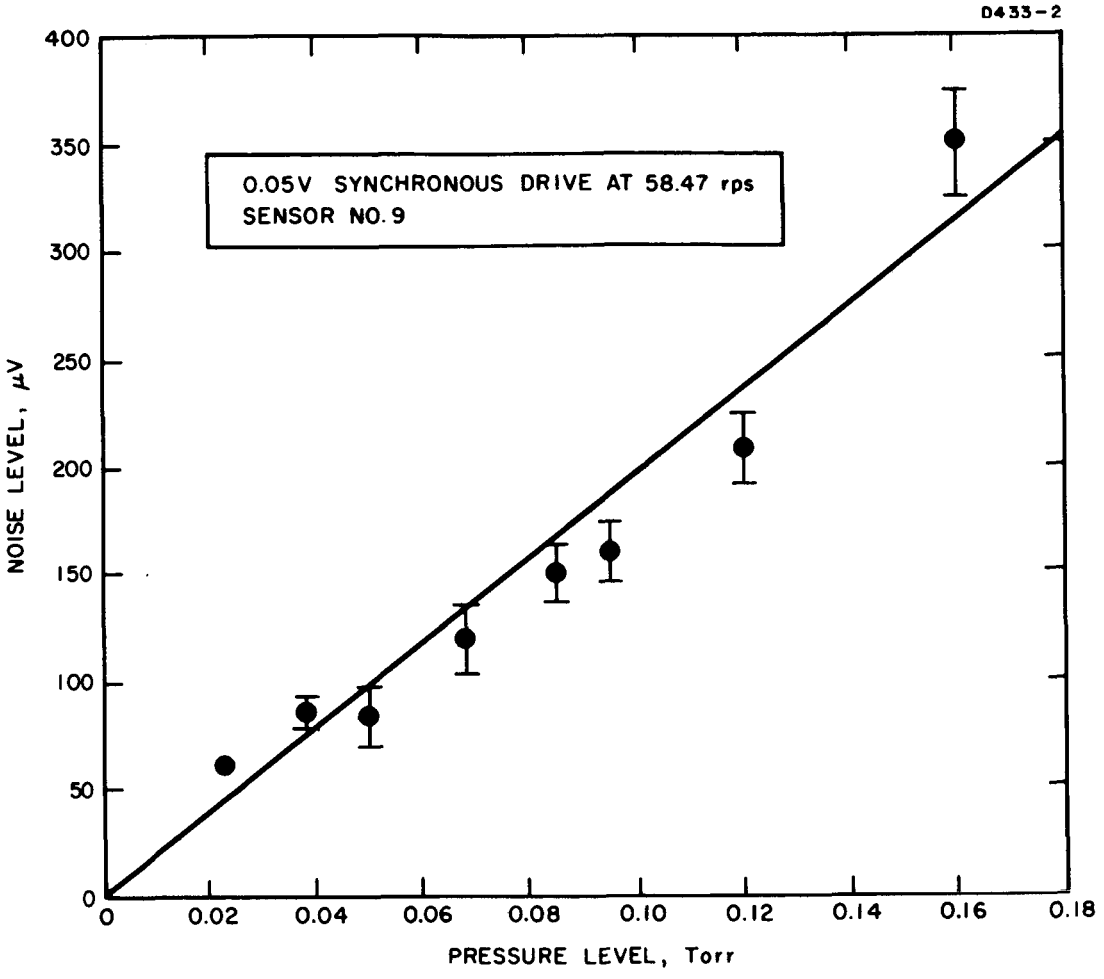

Fig. 11. Pressure dependence of noise.

1. AC Gravitational Gradient Field Generator

The generator of the ac gravitational gradient fields is shown in Fig. 12. The drive unit for the generator is the air bearing support and drive which was originally designed to rotate a sensor structure (see Section II-A of Quarterly Progress Report No. 3). The bearing table supports an aluminum mass holder with four holes 5.0 cm in diameter and 3.5 cm deep, on a radius of 4.0 cm. Opposite pairs of holes can be filled with either aluminum, brass, or tungsten slugs which slip fit into the holes. The various pairs of mass slugs were trimmed so that static and dynamic balance of the generator was achieved even though the mass holder has a mass quadrupole moment. When balanced, the motor is silent under all combinations of speed and mass quadrupole loading, except for the slight, high frequency hiss of the support air passing through the bearing. The motor can be operated either in a synchronous drive mode or a phase locked asynchronous mode using the asynchronous drive described in Section II-A of this report. The readout of the generator rotation speed and phase is obtained through a photoelectric pickoff which reads paint marks on the rotor. This photoelectric signal is used as the reference signal for the lock-in amplifier, and in the asynchronous mode can also be used to supply pulses for the asynchronous drive controller.

The masses of the various slugs used are

Tungsten	1212.0 g
Brass	606.0 g
Aluminum	200.0 g

If four aluminum slugs are used, the generator has no mass quadrupole moment. The maximum mass quadrupole moment of

$$2md^2 = 3.8 \times 10^4 \text{ g cm}^2$$

is obtained when two tungsten slugs are used and the other two holes are left empty. When the opposing pair of holes is filled, the effective mass is just the mass difference. The various combinations possible with our present setup are listed below.

Holes 1 and 3	Holes 2 and 4	Effective Mass (g)
Tungsten	Empty	1212.0
Tungsten	Aluminum	1012.0
Tungsten	Brass	606.0
Brass	Empty	606.0
Brass	Aluminum	406.0
Aluminum	Empty	200.0
Aluminum	Aluminum	0.0

M4181

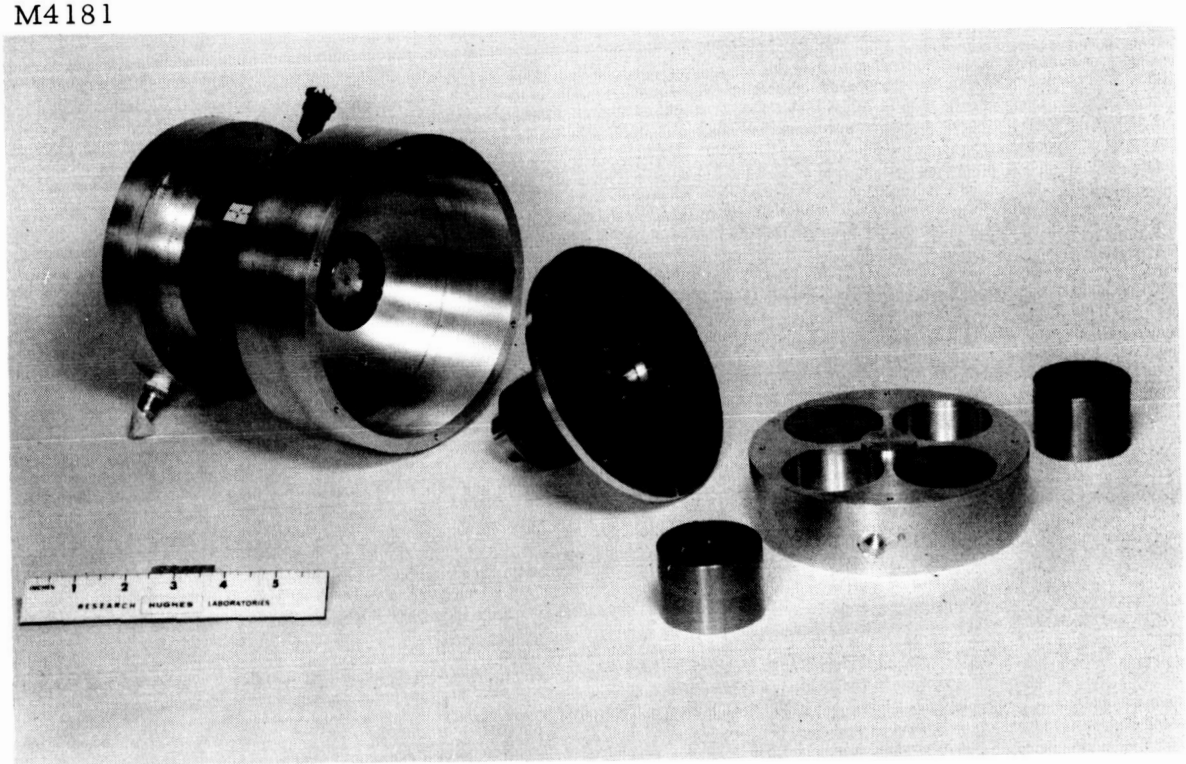

Fig. 12. AC gravitational gradient field generator.

The generator rotates at a nominal speed of 44 rps (2640 rpm); because of the bilateral or tensorial character of the mass quadrupole generators, the ac gravitational gradient fields generated are at 88 Hz, or twice the rotation frequency.

2. Sensor

The sensor used in this first test was one of the adjustable sensors (see Fig. 13; see also Section II-D of Quarterly Progress Report No. 3) which was made to resonate at 88 Hz. A pair of sensor transducers were reversed from that shown in Fig. 13 so that opposing pairs of transducers would produce a differential output voltage which could be fed into the differential input of a Princeton Applied Research HR-8 Lock-in Amplifier.

The sensor was suspended from a spring inside a sensor vacuum chamber (see Fig. 9 of Quarterly Progress Report No. 1), and the evacuated chamber was suspended above the generator by springs attached to the ceiling. A 1/4 in. thick iron plate was suspended between the generator and sensor to provide acoustic and electromagnetic shielding. The completed test setup, except for a cardboard draft shield, is shown in Fig. 14.

The sensor has a resonant frequency of 88.25 Hz, a Q of 106.5, and an arm length of ℓ = 5.0 cm. Under the influence of a gravitational force gradient of $\Gamma \sin 2\Omega t$, the arms respond with a vibrational amplitude of

$$\Delta = \frac{Q\ell}{(2\Omega)^2} \Gamma \cos 2\Omega t = 1.7 \times 10^{-3} \text{ cm/sec}^2 \Gamma \cos 2\Omega t$$

(see Section III-B of Quarterly Progress Report No. 3).

The readout of the sensor vibrations is accomplished by sensing the dynamic strains of the sensor arms with barium titanate strain transducers. The dynamic strain in the arms near the hub corresponding to the mode vibration amplitude Δ is given by

$$\epsilon = \frac{(b + L)\, c}{(L^3/3 + bL^2 + b^2L)} \Delta = 0.026 \text{ cm}^{-1} \Delta$$

where b = 0.3 cm is the radius of the end mass, L = 1.8 cm is the length of the arm, and c = 0.038 cm is the half thickness of the arm.

M 4131

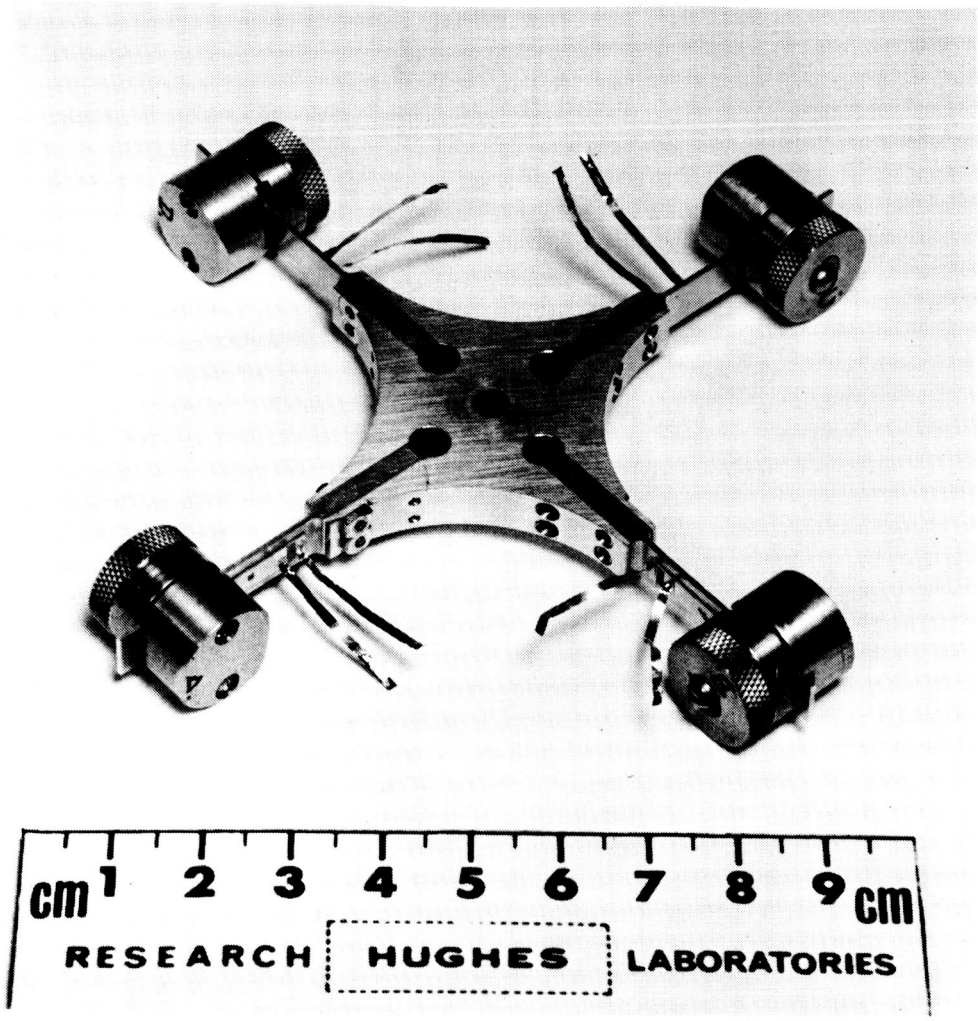

Fig. 11. Adjustable sensor.

M4611

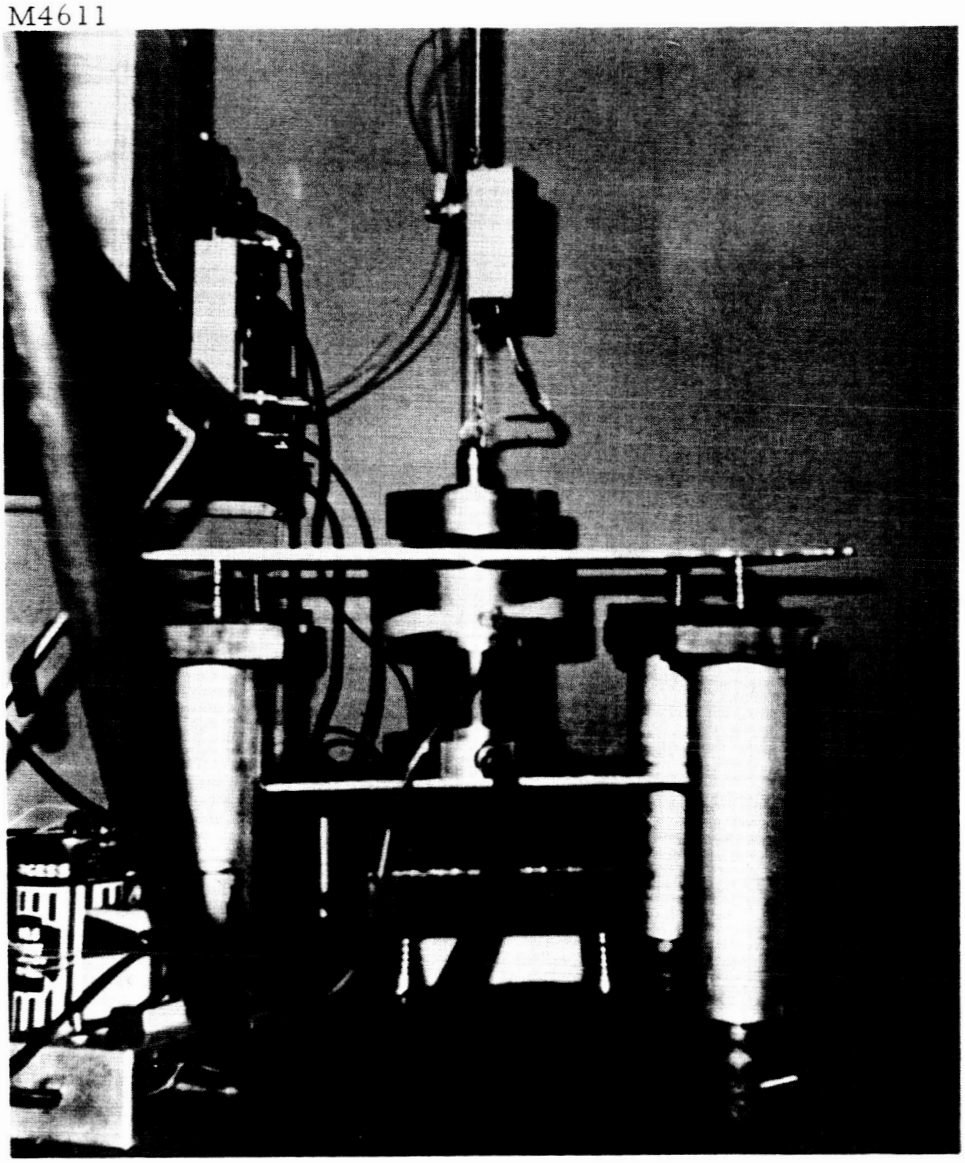

Fig. 14. Relative position of generator and detector.

The barium titanate strain transducers extend over a considerable portion of the arm; therefore, they measure an averaged value of the strain, which is a maximum at the hub and zero at the end. This average measured strain was estimated as

$$\epsilon_t = 0.6\,\epsilon = 0.016\ \text{cm}^{-1}\ \Delta \quad .$$

The transducers used on the sensor had been calibrated on a test setup which compared them with a resistive strain gauge using pure longitudinal strains at 1600 Hz. The transducer factor obtained under these conditions was about $\sigma = 0.7 \times 10^5$ V/unit strain. Thus the voltage output expected from this sensor is

$$V = \sigma\epsilon_t = 1.1 \times 10^3\ \text{V/cm}\ \Delta = 1.85\ \text{V/sec}^2\ \Gamma \cos 2\Omega t \quad .$$

3. Nongravitational Coupling

It is obvious that in order to detect the very weak ac gravitational forces being generated by the rotating mass quadrupole, the generator and sensor must be well shielded from each other to prevent acoustic and electromagnetic coupling. The sensor is highly sensitive to acoustic noise with a frequency component at its resonance frequency, but experience has shown that the acoustic noise can be eliminated by placing the sensor in a vacuum chamber at a few milliTorr.

Although an ideal sensor is theoretically insensitive to vibrations of the mounting structure (see Appendix of Quarterly Progress Report No. 3), in practice a small amount of the vibrations in the sensor mount leak into the gradient sensing mode. Because of this, an effort must be made to keep the sensor mount vibrations at a low level. This was accomplished by suspending the sensor from the chamber by a spring, and the chamber from the ceiling by another spring. The generator was isolated from the workbench by compression springs, and the iron shield plate was vibrationally isolated from both the generator and sensor by its own support springs (see Fig. 14).

Electromagnetic coupling can occur in two ways: (1) by direct interaction of the rotating magnetic fields of the motor with the arms of the sensor; (2) by stray electromagnetic voltages or currents entering the sensor output leads or the preamplifier. The electromagnetic coupling into the output electronics is easily checked, since it is independent of the resonant response of the sensor and was found to be unobservable even in the single ended mode of operation, although all data were taken with a differential input to insure that pickup was not a problem.

Direct coupling of the rotating magnetic fields around the generator motor into the sensor was found to be a major problem. At first it was not well understood, since the sensor arms were of aluminum and the sensor masses of brass. This interaction was originally eliminated by using a phase locked asynchronous drive invented by Larry R. Miller (see Section II-A of this report). In this mode of operation of the generator, the generator motor is driven by currents at some higher frequency, typically 200 Hz, so they do not excite the sensor mode. The amplitude of the drive voltage is controlled by a servo loop so that the rotor remains at a constant speed of 44 rps. The servo loop is so tight that both the frequency and the phase of the rotor are held tightly to the phase of a reference signal from a precise oscillator (General Radio Frequency Synthesizer). It was later discovered that the sensor had been assembled with stainless steel screws; when they were replaced by brass screws, the magnetic coupling was eliminated and it was possible to take the data using synchronous drive on the generator.

One important factor aided greatly in the problem of eliminating the nongravitational coupling between the generator and the sensor. Because of the double mass in the mass quadrupole, the generator is rotated at half of the sensor frequency. Therefore, predominantly all of the acoustic and electromagnetic energy produced by the generator is at a frequency which is outside the sensor response frequency; only that small portion of the energy which is harmonically generated at twice the rotation frequency must be shielded against.

The generator was designed specifically for the problem of determining the nongravitational coupling effects. If four aluminum slugs are put in the mass holder, the generator has no time varying mass quadrupole moment and therefore no ac gravitational gradient field; however, it still retains all of its electromagnetic and acoustic properties. A test run was made at 5 cm separation distance using the four aluminum slugs. The generator speed was varied from 43 to 45 rps, so that the sensor mode frequency of 88 Hz was not missed. The sensor output remained at 0 ± 4 nV. The rotor was then deliberately unbalanced so that the acoustic output was noticeably increased and the test was rerun, with the same results. These experiments demonstrated that the response of the sensor structure and sensor electronics to nongravitational forces arising from all sources, including the generator, was less than 4 nV.

4. Gravitational Coupling

After the test for nongravitational coupling, two of the aluminum slugs were replaced with tungsten slugs, resulting in a mass difference of 1012 g. The rotor was rebalanced and the generator and detector were placed 5 cm apart. The theoretical calculations presented

in Section III-B of this report indicate that at this distance, and with this size sensor, a 1012 g effective mass should produce an equivalent gravitational force gradient of

$$\Gamma = 1.25 \times 10^{-7} \sin 2\Omega t \qquad \text{sec}^{-2} \quad .$$

This ac gradient has an amplitude of about 1/20 of the earth's gravitational force gradient. From the theory of operation of the sensors, this gradient should cause the gravitational gradient sensing mode of the detector to oscillate with an amplitude

$$\Delta = 2.15 \times 10^{-10} \cos 2\Omega t \qquad \text{cm} \quad .$$

Although the amplitude of these motions is extremely small, of the order of 1/100 of the diameter of an atom, they are easily measured if piezoelectric strain transducers are used. Similar sensing techniques used on the gravitational radiation detectors at the University of Maryland have measured motions down to 10^{-14} cm.

The motion induced in the sensor causes an average strain in the arms of

$$\epsilon_t = 3.3 \times 10^{-12} \cos 2\Omega t \quad .$$

If we assume that the transducer calibration is $\sigma = 0.7 \times 10^5$ V/strain, the predicted output of these sensors under excitation by a generator with a 1 kg mass difference at a 5 cm separation distance would be

$$V = \sigma\epsilon_t = 230 \cos 2\Omega t \qquad \text{nV}$$

or an rms voltage of 160 nV.

When the test was run, the actual measured output voltage of the sensor under these conditions was 104 ± 8 nV (rms). This is much larger than the output voltage fluctuations of 4 nV under the control conditions using the four aluminum masses, and is slightly less than the predicted output. The exact reason for this lower output is not known, but it is assumed that it is a result of the difficulty in obtaining an accurate calibration of the strain transducers.

Further effort will be devoted to insuring that the voltage output seen was caused only by gravitational gradient coupling. Data will be taken as a function of distance, orientation, phase, frequency, and mass quadrupole moment on various types of sensors, and will be compared with the theoretical predictions. When this work is completed, a paper will be prepared and submitted for publication.

We do not doubt, however, that we have observed a gravitational gradient coupling between the generator and the sensor. We feel that we have demonstrated that these gravitational mass sensor structures and our present transducer-amplifier-recorder systems are more than adequate for the purpose of detecting gravitational force gradients as small as 1/20 of the earth's gradient and that our sole remaining problem for this research phase of the present contract is a continued effort to reduce the noise leaking into the sensor mode under rotating conditions to the point where the signals due to the earth's gravitational gradient can be seen.

III. THEORETICAL PROGRAM

A. Gravitational Interactions Between a Sensor and a Rotating Mass Quadrupole

The model which we will use to calculate the gravitational interaction between a rotating mass quadrupole and a resonant cruciform gravitational mass sensor is shown in Fig. 15. The generator is assumed to be two spherical masses of mass M separated by a distance 2d and rotated about their center of mass at a constant angular frequency $\dot{\theta} = \Omega$. The detector is assumed to be four spherical masses of mass m on orthogonally disposed massless arms of length ℓ. The sensor is supported from above so that its center of mass is at a height h directly above the center of mass of the generator. The particular mode of the sensor used to sense the gravitational gradient forces is the dual tuning fork mode (see Fig. 16). It was shown in previous analyses (Appendix of Quarterly Progress Report No. 3) that this mode does not respond to vibrational forces at the mount nor to the direct gravitational force field, but only to the gradient of the gravitational force field.

The forces on the sensor resulting from the gravitational interaction between the rotating masses M and the sensor masses m typically consist of

$$F_i = \frac{G\,M\,m}{R_i^2} \qquad i = 1 \text{ to } 4$$

where

$$R_i^2 = h^2 + r_i^2$$

and

$$r_1^2 = \ell^2 + d^2 - 2\ell d \cos\theta$$

$$r_2^2 = \ell^2 + d^2 + 2\ell d \cos\theta$$

$$r_3^2 = \ell^2 + d^2 - 2\ell d \sin\theta$$

$$r_4^2 = \ell^2 + d^2 + 2\ell d \sin\theta$$

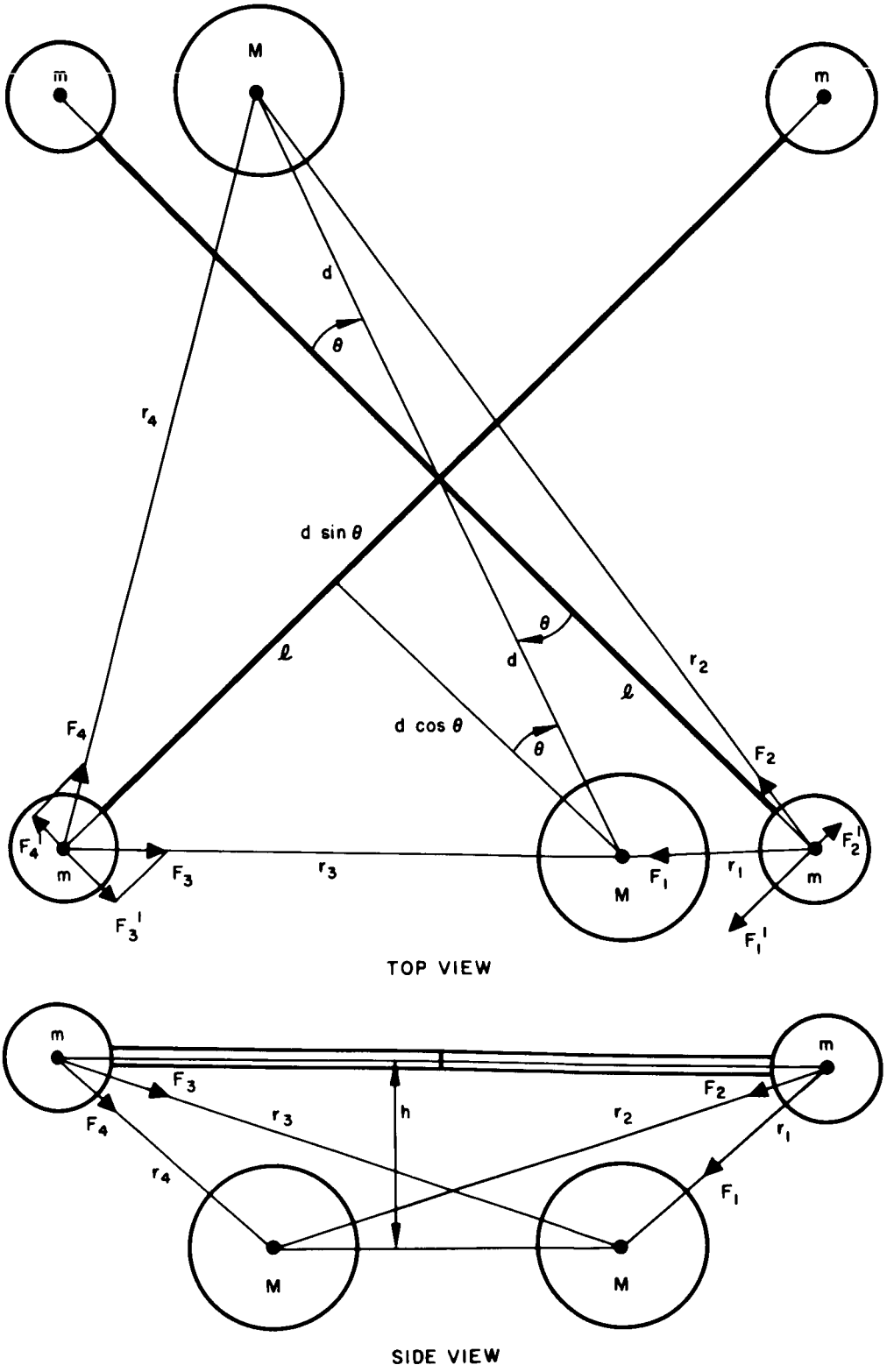

Fig. 15. Model for gravitational interaction calculation.

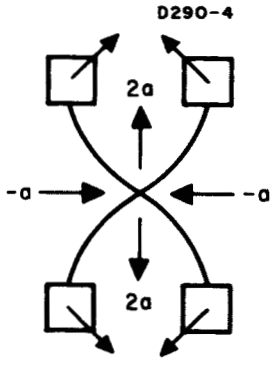

Fig. 16.

Gravity gradient sensing mode.

However, the component of the forces which drive the sensing mode of the detector are the tangential components of the forces F_i

$$F_1' = \frac{G\ M\ m}{R_1^3}\ d \sin\theta$$

$$F_2' = \frac{G\ M\ m}{R_2^3}\ d \sin\theta$$

$$F_3' = \frac{G\ M\ m}{R_3^3}\ d \cos\theta$$

$$F_4' = \frac{G\ M\ m}{R_4^3}\ d \cos\theta$$

The resultant force on each of the arms as a result of the tangential components of the forces F_i' is given by

$$F = 1/2 \left[(F_1' - F_2') + (F_3' - F_4')\right]$$

$$= \frac{G\ Mmd}{2}\left[\left(\frac{1}{R_1^3} - \frac{1}{R_2^3}\right) \sin\theta + \left(\frac{1}{R_3^3} - \frac{1}{R_4^3}\right) \cos\theta\right] .$$

Because R_i is a function of the angle θ, the resultant force F has a complex behavior with the angle of rotation. To calculate the components of the resultant force as a function of frequency, we will expand the terms in R_i^{-3}. Letting

$$R^2 = \ell^2 + d^2 + h^2,$$

we can write the resultant force F as

$$F = \frac{G\ Mmd}{2}\left\{\left[(R^2 - 2\ell d \cos\theta)^{-3/2} - (R^2 + 2\ell d \cos\theta)^{-3/2}\right] \sin\theta + \left[(R^2 - 2\ell d \sin\theta)^{-3/2} - (R^2 + 2\ell d \sin\theta)^{-3/2}\right] \cos\theta\right\} .$$

Bringing R^2 out from the denominator and letting $\Lambda = \frac{\ell d}{R^2}$, we obtain

$$F = \frac{G\,Mmd}{2R^3}\left\{\left[(1 - 2\Lambda\cos\theta)^{-3/2} - (1 + 2\Lambda\cos\theta)^{-3/2}\right]\sin\theta + \left[(1 - 2\Lambda\sin\theta)^{-3/2} - (1 + 2\Lambda\sin\theta)^{-3/2}\right]\cos\theta\right\}$$

We now expand each term using the binomial expansion theorem; however, because the expansion parameter Λ can be as high as $1/3$ when the generator and detector are separated by 4.5 cm, it is necessary to take the expansion out to the seventh order.

$$F = \frac{G\,Mmd}{2R^3}\left\{\left[6\Lambda\cos\theta + 35\Lambda^3\cos^3\theta + \frac{693}{4}\Lambda^5\cos^5\theta + \frac{6435}{8}\Lambda^7\cos^7\theta\right]\sin\theta + \left[6\Lambda\sin\theta + 35\Lambda^3\sin^3\theta + \frac{693}{4}\Lambda^5\sin^5\theta + \frac{6435}{8}\Lambda^7\sin^7\theta\right]\cos\theta\right\}$$

The even order terms drop out because of the symmetry. If we rearrange the above equation and use the trigonometric identities

$$\begin{aligned} 2\sin\theta\cos\theta &= \sin 2\theta \\ 2(\cos^3\theta\sin\theta + \sin^3\theta\cos\theta) &= \sin 2\theta \\ 16(\cos^5\theta\sin\theta + \sin^5\theta\cos\theta) &= 5\sin 2\theta + \sin 6\theta \\ 32(\cos^7\theta\sin\theta + \sin^7\theta\cos\theta) &= 7\sin 2\theta + 3\sin 6\theta, \end{aligned}$$

we can obtain the expression

$$F = \frac{3\,G\,Mm\ell d^2}{R^5}\left\{\left(1 + \frac{35}{12}\Lambda^2 + \frac{1155}{128}\Lambda^4 + \frac{15015}{512}\Lambda^6\right)\sin 2\Omega t + \left(\frac{231}{128}\Lambda^4 + \frac{6435}{512}\Lambda^6\right)\sin 6\Omega t\right\}$$

where we brought out a factor of $6\Lambda = 6\ell d/R^2$ from behind the brackets. This expression shows that the interaction force between the generator and detector is complicated at close distances of separation and depends upon the sizes of the generator and detector, as well as the separation distance.

In order to relate these forces to the previous work, we define an equivalent gravitational force gradient by the relation

$$\Gamma = \frac{F}{m\ell}$$

where m is the mass and ℓ is the length of a sensor arm.

The effective gravitational force gradient was computer calculated for various values of the separation distance h, and the results for the amplitudes of the two frequency components are plotted in Fig. 17. For this curve it was assumed that the sensor had an effective radius of 5 cm, and the generator consisted of two 1 kg masses on a radius of 4 cm. At distances greater than 12 cm, the only important term is the first; and the effective gravitational gradient is given by the formula

$$\Gamma = \frac{3\,G\,M\,d^2\,\sin 2\Omega t}{(h^2 + d^2 + \ell^2)^{5/2}}$$

At the nominal separation distance of 5 cm the effective gravitational force gradient resulting from the generator is $1.24 \times 10^{-7}\ \text{sec}^{-2}$. This is about 1/20th of the earth's gradient. These two 1 kg masses have a large gradient because we are able to bring the sensor very close to them.

B. Rotating Sensor Mode Analysis

The interference effects between the two translational modes formed by the spring constant of the torsion wire mount acting against the total sensor mass and the two translational modes of the sensor head itself were analyzed in Quarterly Progress Report No. 4. The effect of rotation on the vibrational modes of the sensor alone was also analyzed.

The two analyses have been combined, and vibrational mode frequency solutions were obtained for a sensor on a torsion wire mount as a function of rotation speed. The analysis and comparison with the experimental data was prepared as a paper and is included as the Appendix to this report.

Since we now have a complete solution for the behavior of an ideal sensor which agrees well with the experimental data, it is possible to study the effects of errors in construction as perturbations on the ideal sensor behavior. As was pointed out in Appendix to Quarterly Progress Report No. 3, the gravitational gradient sensing mode of an ideal sensor is not excited by external vibrations on the mount. It is quite probable that a nonideal sensor will allow a small portion of the external vibrational forces to leak into the gravitational gradient sensing mode. An analysis is now in progress which assumes that the sensor masses and arm lengths can be different and that the sensor may not be held at its center of mass. Vibrational forces and torques of various frequencies will be assumed to be applied at the rotation axis to determine whether the gravity sensing mode is excited. This work probably will have to be done on the analog computer at Culver City.

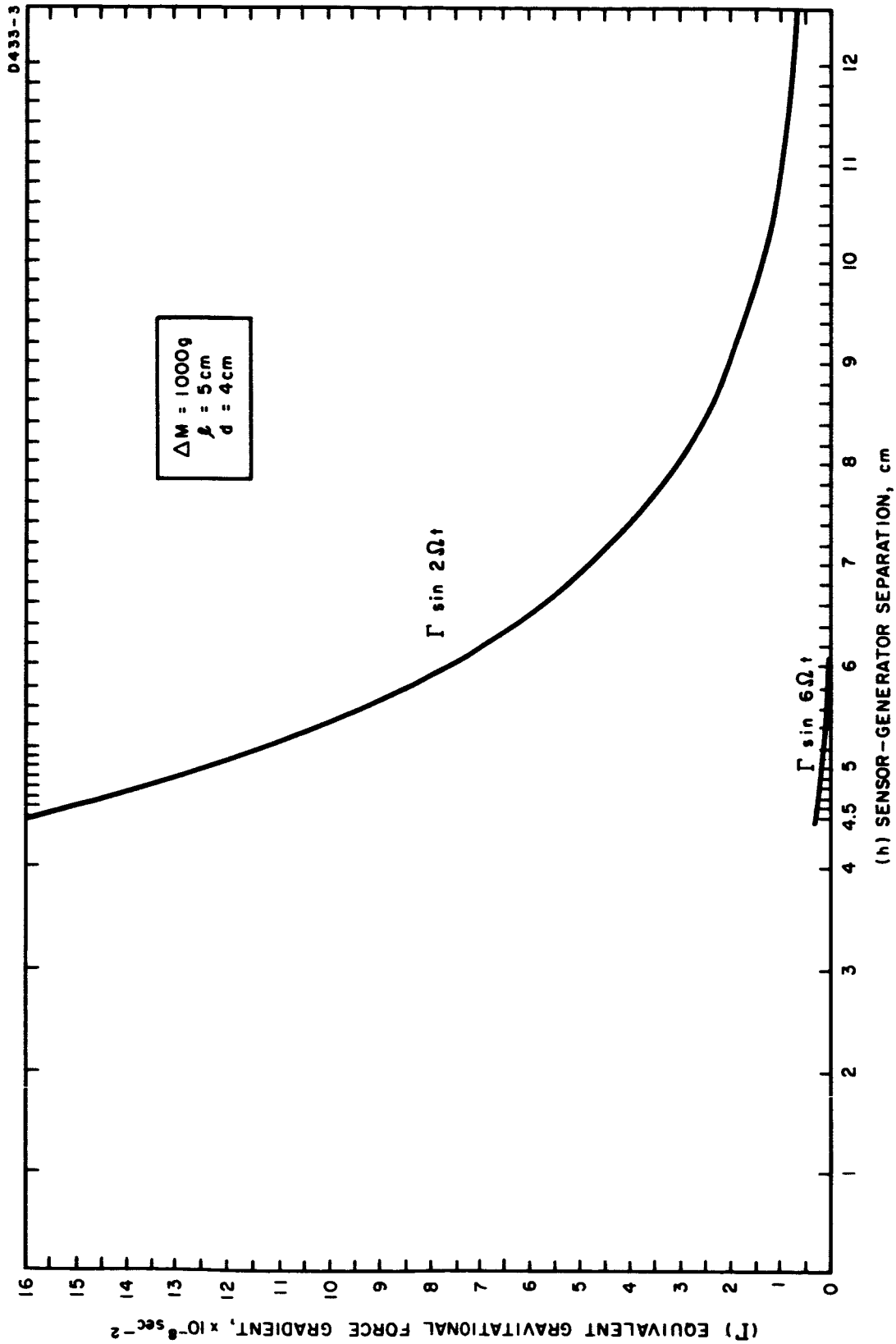

Fig. 17. Calculated equivalent gravitational force gradient.

IV. CONCLUSIONS

The experimental work on the generation and detection of ac gravitational gradient fields has demonstrated that the gravitational mass sensor structures and transducer-amplifier-recorder systems which we are presently using are more than adequate for the purpose of detecting gravitational force gradients as small as 1/20 of the earth's gradient. Our sole remaining problem for the research phase of this contract is a continued effort to reduce the noise leaking into the sensor mode under rotating conditions to the point where signals from the earth's gravitational gradient can be seen.

The noise tests on rotating sensors gave a noise level of 60 μV. The gravitational gradient signals expected are about 4 μV, or about 7% of this noise level. The major source of noise at the present time is air turbulence which excites the sensor as it rotates through the residual air in the vacuum chamber. A co-rotating sensor chamber would have eliminated this source of noise; however, it could not be used during the tests because it was incompatible with the present sensor mounting structure.

The analysis of the sensor vibrational mode frequencies under rotation has given us some design data which will be used in the design of an optimum sensor mount and optimum sensor structure.

V. RECOMMENDATIONS

It is recommended that the following investigations be continued:

- Experimental investigation of noise in bearings and drives
- Experimental investigation of sensor mounts
- Theoretical investigation of the effects of errors in construction on sensor response to external noise sources.

APPENDIX

VIBRATIONAL MODE BEHAVIOR OF ROTATING GRAVITATIONAL GRADIENT SENSORS*

*To be presented at the AIAA/JACC Guidance and Control Conference, Seattle, Washington, 15 to 17 August 1966.

ABSTRACT

We are engaged in a program to design and construct a feasibility model of a gravitational mass sensor that uses a rotating resonant elastic system to detect the gravitational force gradient fields of the mass. As part of this program, we have carried out a detailed analysis of the vibrational mode behavior of a rotating cruciform shaped spring-mass system supported on a spring mount. The behavior of the sensor modes as a function of the design parameters and the rotation speed agrees well with data obtained from actual sensors used in the experimental portion of the work. This theory can aid in the design of optimum sensors and sensor mount structures.

PROGRAM OBJECTIVES

The ultimate objective of our work on gravitational mass sensors is to develop a small, lightweight, rugged graviational gradient sensor to be used on lunar orbiters to measure the mass distribution of the moon and on deep space probes to measure the mass of the asteroids. The possible applications,[1,2] the basic concepts,[2-10] and the theoretical limitations[11,12] have been investigated in earlier papers. The purpose of the present research program is to develop and refine experimental techniques for measuring gravitational and inertial fields using rotating elastic systems, and to develop a more complete understanding of these types of sensors so that accurate predictions of sensor behavior can be made which are based on practical system configurations and measured device sensitivity

SUMMARY OF PRIOR WORK

The most promising form of gravitational mass sensor has been found to be a cruciform shaped spring-mass system. A number of different cruciform sensor heads (see, e.g., Fig. 1) have been designed and studied experimentally. They have all demonstrated a basic structural stability under high rotation speed. Effort is now concentrated on reducing the effects of bearing noise on the sensor modes.

A continuing theoretical study of the transversely vibrating cruciform sensor structure is under way. The model used for the analyses consists of a central mass connected to the using vehicle through an elastic mount, four equal sensing masses on transversely vibrating arms, and a sensed mass. The analysis is quite complicated because of the multiplicity of masses and springs, the nonuniform character of the gravitational field, and the requirement that the restoring forces on the sensor arms include the centrifugal force as well as the spring constant of the arms. The results of these analyses[2,11,12] indicate that there is a particular mode of vibration of the sensor – the tuning fork mode (see Fig. 2(a)) – which is at a frequency which differs from that

M 3615

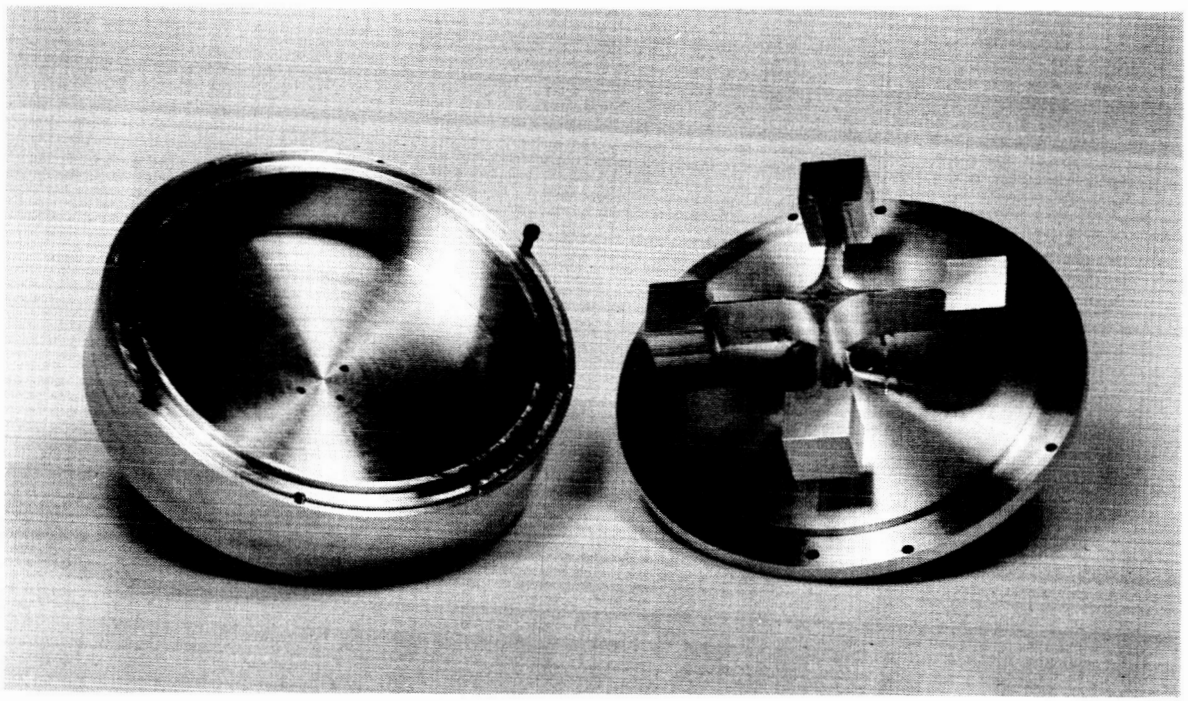

Fig. 1. Five-inch diameter cruciform gravitational mass sensor.

of the other modes, responds to the presence of a gravitational force gradient field when rotated at half of its vibrational frequency and yet does not respond to inertial forces.[12]

Readout of the very small (10^{-10} in.) vibrations expected is accomplished by means of piezoelectric strain transducers attached to the transversely vibrating arms of the cruciform. These barium titanate transducers have a gauge factor of 10^5 V/unit strain and have been used in previous work[13] to measure motions down to 10^{-14} in. Prior analysis has indicated[12] that this gauge sensitivity will yield gravity gradient produced signals of the order of a few microvolts. Since this is a narrow-band signal at 100 Hz, it is easily measured with a low noise tuned amplifier, such as the General Radio Tuned Amplifier 1232A, which has an equivalent input noise voltage of 50 nV.

STATEMENT OF PROBLEM

A major problem with cruciform gravitational mass sensors lies in maintaining adequate frequency separation between the various vibration sensitive resonant modes of the sensor system and the gradient sensing mode of the cruciform sensing head. If this frequency separation can be maintained, it will then be possible to use narrow band amplifiers to separate the gravitationally driven sensor response from the inertially driven responses.

In earlier work,[12] it was found that if the sensor has a small central mass and is well isolated from other masses by suspension from a weak spring, the gravity gradient sensing mode is the lowest in frequency and is well separated from the rest of the vibrational modes. However, when rotation of the sensor is attempted while using a mount with a weak spring constant, it is not possible to rotate the sensor up to the desired operating speed because the mount cannot resist the centrifugal forces. When the mount stiffness is increased so that it can resist the centrifugal force, two new translational modes formed by

the spring constant of the mount and the total mass of the sensor become important. These modes cause the two translational modes in the sensor head to shift upward, helping to solve the mode separation problem. However, under rotation, the translational modes split; at the desired rotational speed, they become close enough to the gradient sensing mode to make frequency selection techniques difficult.

In an attempt to understand this behavior, an analysis of vibrational mode behavior under rotation was undertaken. This analysis was then compared with the experimental data.

THEORY OF ROTATING CRUCIFORM SENSORS

As a result of earlier theoretical and experimental work,[11, 12] it has long been known that the cruciform shaped gravitational mass sensors have four primary oscillation modes which involve the spring constant of the bending arms. These are the gradient sensing or tuning fork mode (Fig. 2(a)), a torsional mode (Fig. 2(b)) and two translational modes (Fig. 2(c)). In addition, there are higher order harmonics of these four basic modes as well as other modes of oscillation involving other elastic properties of the cruciform, such as the torsional or longitudinal spring constants. These higher order modes, as well as the torsional mode, are usually at much higher frequencies than the gradient sensing mode and the two translational modes; they cause relatively little difficulty since they can be easily filtered out.

Since we wished to investigate the vibrational mode behavior of this class of sensors in as rigorous a manner as possible, the model used was not that of one of the actual sensors, but was chosen to be as general as possible while still retaining the important features of the actual sensors. The model (Fig. 3) assumes a central mass M and four smaller masses m at the ends of four arms of length a ; these arms are pivoted at a distance b from the center of the sensor. The central mass is assumed to be attached to a rotating axis through an axially symmetric spring of spring constant K. (The model shows four

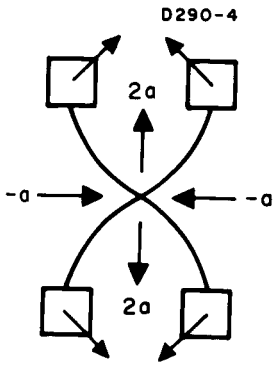

(a)

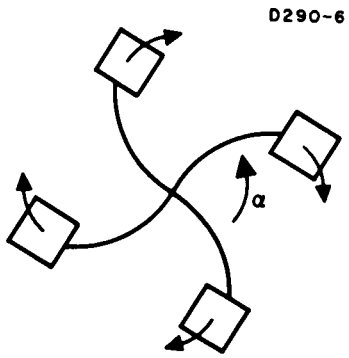

(b)

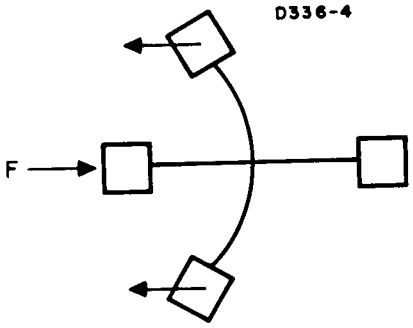

(c)

Fig. 2. Sensor vibrational modes

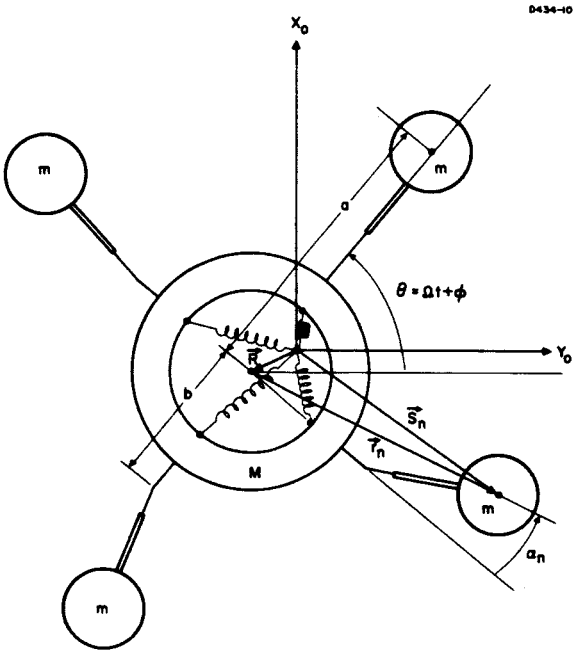

Fig. 3. Model of rotating cruciform sensor on spring mount.

coil springs; the experiment used a flexible shaft.) To simplify the analysis the axis was assumed to remain fixed in position at the origin of the inertial reference frame, while rotating at a constant angular frequency of Ω. The central mass M, since it is attached to the rotating axis through springs, is not constrained to the origin but its center of mass is in general at the position $\vec{R}$ and its speed of rotation varies about Ω by a small amount $\dot{\phi}$ due to the interaction with the vibrating arms. The masses at the ends of the arms participate in the general rotation of the sensor and also can vibrate through a small angle a_n with respect to the rotating reference frame.

The kinetic energy of the system is given by the general formula

$$T = \frac{1}{2} M \dot{\vec{R}}^2 + \frac{1}{2} m \sum_{n=1}^{4} \dot{\vec{s}}_n^{\,2} + \frac{1}{2} I \dot{\theta}^2 \qquad (1)$$

where $\vec{R}$ is the position of the central mass, $\vec{s}_n$ is the position of the n^{th} end mass, I is the moment of inertia of the central mass, and $\dot{\theta} = \Omega + \dot{\phi}$ is its instantaneous angular velocity. We have assumed that the moment of inertia of the end masses is small enough to be neglected.

The potential energy of the system is in the springs of the vibrating arms and the mount

$$V = \frac{1}{2} k a^2 \sum_{n=1}^{4} a_n^2 + \frac{1}{2} K \vec{R}^2 \qquad (2)$$

where k is the effective spring constant of the arms, K is the effective spring constant of the mount, and a_n is the angular deflection of the n^{th} arm. Using these equations, the Lagrangian of the system is therefore

$$L = T - V = \frac{1}{2} M \dot{\vec{R}}^2 + \frac{1}{2} m \sum_{n=1}^{4} \dot{\vec{s}}_n^2$$

$$+ \frac{1}{2} I \dot{\theta}^2 - \frac{1}{2} ka^2 \sum_{n=1}^{4} \alpha_n^2 - \frac{1}{2} K \vec{R}^2 . \qquad (3)$$

For our particular system, the position of the n^{th} arm is given by

$$\vec{s}_n = \vec{R} + \vec{r}_n ; \qquad (4)$$

substituting this into (3) we obtain the Lagrangian in terms of the central mass motion $\vec{R}$ and rotation $\dot{\theta}$, and the relative motion $\vec{r}_n$ and angular deflection α_n of the arms

$$L = \frac{1}{2} (M + 4m) \dot{\vec{R}}^2 + m \dot{\vec{R}} \sum_{n=1}^{4} \dot{\vec{r}}_n + \frac{1}{2} m \sum_{n=1}^{4} \dot{\vec{r}}_n^2$$

$$+ \frac{1}{2} I \dot{\theta}^2 - \frac{1}{2} ka^2 \sum_{n=1}^{4} \alpha_n^2 - \frac{1}{2} K \vec{R}^2 . \qquad (5)$$

This form of the Lagrangian is still not suitable for our purposes, since both $\vec{r}_n$ and $\vec{R}$ are a function of the rotation of the sensor θ as well as the motions of the sensor α_n and x.

The motion of the center of mass of the central mass is given by

$$\vec{R} = (x \cos \theta - y \sin \theta) \vec{1}_x + (x \sin \theta + y \cos \theta) \vec{1}_y \qquad (6)$$

where $\theta = \Omega t + \phi$ is the instantaneous rotation of the central mass and $\vec{1}_x$ and $\vec{1}_y$ are unit vectors.

To first order in x and ϕ, the velocity of the center of mass is given by

$$\dot{\vec{R}} = [(\dot{x} - \Omega y)\cos\Omega t - (\dot{y} + \Omega x)\sin\Omega t]\,\vec{l}_x + [(\dot{x} - \Omega y)\sin\Omega t + (\dot{y} + \Omega x)\cos\Omega t]\,\vec{l}_y \tag{7}$$

and the square of the velocity by

$$\dot{\vec{R}}^2 = \dot{x}^2 + \dot{y}^2 + 2\Omega(x\dot{y} - \dot{x}y) + \Omega^2(x^2 + y^2) = (\dot{x} - \Omega y)^2 + (\dot{y} + \Omega x)^2 \tag{8}$$

where we have assumed that $\theta \approx \Omega t$ and that products of order $x^2\phi$ and $\phi^2 x$ are negligible.

The position of the n^{th} end mass is given by

$$\vec{r}_n = r_n\left[\vec{l}_x \cos\left(\theta + \frac{n\pi}{2} + \alpha_n\right) + \vec{l}_y \sin\left(\theta + \frac{n\pi}{2} + \alpha_n\right)\right] \tag{9}$$

where the absolute value of the effective length of the sensor arm is given by

$$r_n = a\left(1 - \frac{1}{2}\,\frac{b}{a-b}\,\alpha_n^2\right) \equiv a - \frac{1}{2}\,aB\alpha_n^2 \tag{10}$$

where a is the nominal length of the arm and b is the distance from the effective pivot point of the arm to the center of the sensor, $B = \frac{b}{a-b}$ is chosen so that $B = 0$ and $r_n = a$ when the arm is pivoted at the center of rotation ($b \approx 0$) and B and r_n become indeterminant when the arm is pivoted at the end ($b \approx a$).

The calculation of $\Sigma\dot{\vec{r}}_n$ and $\Sigma\dot{\vec{r}}_n^2$ in terms of θ and α_n is straightforward but tedious. For the sum of the arm velocities we obtain

$$\frac{1}{a}\sum_{n=1}^{4}\dot{\vec{r}}_n = [(\dot{a}_3 - \dot{a}_1) - \Omega(a_4 - a_2)]\,[\vec{1}_x \cos\Omega t + \vec{1}_y \sin\Omega t]$$

$$- [(\dot{a}_4 - \dot{a}_2) + \Omega(a_3 - a_1)]\,[\vec{1}_x \sin\Omega t + \vec{1}_y \cos\Omega t] \qquad (11)$$

where we kept only terms of first order in a and ϕ, since we will later be multiplying (11) by the center of mass velocity (7). For the relative energy of the arms alone, we obtain

$$\frac{m}{2}\sum_{n=1}^{4}\dot{\vec{r}}_n^{\,2} = 2ma^2\dot{\theta}^2 + ma^2\dot{\theta}\sum_{n=1}^{4}\dot{a}_n$$

$$+ \frac{1}{2}ma^2\sum_{n=1}^{4}\dot{a}_n^{\,2} - \frac{1}{2}ma^2 B\Omega^2\sum_{n=1}^{4}a_n^{\,2} \qquad (12)$$

where we have kept terms of second order in a and ϕ.

Combining (7), (8), (11), and (12) into (5), we obtain the Lagrangian in terms of the motions and rotation of the central mass and the relative angular displacement of the arms

$$L = \frac{1}{2}(M + 4m)[(\dot{x} - \Omega y)^2 + (\dot{y} + \Omega x)^2] + ma\Big\{(\dot{x} - \Omega y)[(\dot{a}_3 - \dot{a}_1) - \Omega(a_4 - a_2)]$$

$$+ (\dot{y} + \Omega x)[(\dot{a}_4 - \dot{a}_2) + \Omega(a_3 - a_1)]\Big\} + \frac{1}{2}(I + 4ma^2)\dot{\theta}^2 + ma^2\dot{\theta}\sum_{n=1}^{4}\dot{a}_n$$

$$+ \frac{1}{2}ma^2\sum_{n=1}^{4}\dot{a}_n^{\,2} - \frac{1}{2}(ka^2 + ma^2 B\Omega^2)\sum_{n=1}^{4}a_n^{\,2} - \frac{1}{2}K(x^2 + y^2)$$

(13)

where we have neglected terms of third order in x, y, a_n, and ϕ.

This form of the Lagrangian contains the description of the behavior of the sensor in terms of the angular displacement α_n of each one of the arms. However, since we are interested in the behavior of the vibrational modes of the sensor, it will simplify things if we express the Lagrangian in terms of the equivalent displacement of the vibrational modes. Each mode of vibration corresponds to a particular combination of arm phase and amplitude. The four primary modes of interest are the gravity gradient sensing mode (see Fig. 2(a))

$$A_g = \frac{a}{2} (\alpha_1 - \alpha_2 + \alpha_3 - \alpha_4) \ , \tag{14}$$

the torsional mode (see Fig. 2(b))

$$A_t = \frac{a}{2} (\alpha_1 + \alpha_2 + \alpha_3 + \alpha_4) \ , \tag{15}$$

and the two orthogonal translational modes (see Fig. 2(c))

$$A_+ = \frac{a}{\sqrt{2}} (\alpha_3 - \alpha_1) \tag{16}$$

$$A_- = \frac{a}{\sqrt{2}} (\alpha_4 - \alpha_2) \ . \tag{17}$$

The two translational modes can also be expressed in terms of right and left handed circulating translational modes which are complex combinations of the orthogonal modes

$$A_r = \frac{1}{\sqrt{2}} (A_+ + iA_-) = \frac{a}{2} (-\alpha_1 - i\alpha_2 + \alpha_3 + i\alpha_4) \tag{18}$$

$$A_\ell = \frac{1}{\sqrt{2}} (A_+ - iA_-) = \frac{a}{2} (-\alpha_1 + i\alpha_2 + \alpha_3 - i\alpha_4) \tag{19}$$

where the complex number i indicates a 90^{o} phase lag in the response of the arm vibrating in that particular mode.

It is obvious from inspection that

$$a^2 \sum_{n=1}^{4} a_n^{\,2} = a^2(a_1^{\,2} + a_2^{\,2} + a_3^{\,2} + a_4^{\,2}) = A_g^{\,2} + A_t^{\,2} + A_+^{\,2} + A_-^{\,2}$$

$$= A_g^{\,2} + A_t^{\,2} + A_r^{\,2} + A_\ell^{\,2} \qquad (20)$$

and that

$$a \sum_{n=1}^{4} \dot{a}_n = 2\,\dot{A}_t \qquad (21)$$

so that the Lagrangian (13) in terms of the amplitudes of the normal mode vibrations is given by:

$$L = \frac{(M + 4m)}{2m}\left[(\dot{x} - \Omega y)^2 + (\dot{y} + \Omega x)^2\right] + \sqrt{2}(\dot{x} - \Omega y)\left[\dot{A}_+ - \Omega A_-\right]$$

$$+ \sqrt{2}\,(\dot{y} + \Omega x)\,\left[\dot{A}_- + \Omega A_+\right] + \frac{1}{2}\left(\frac{I + 4ma^2}{m}\right)\dot{\theta}^{\,2} + 2a\dot{\theta}\dot{A}_t$$

$$+ \frac{1}{2}\,(\dot{A}_g^{\,2} + \dot{A}_t^{\,2} + \dot{A}_+^{\,2} + \dot{A}_-^{\,2}) - \frac{1}{2}\left(\frac{k}{m} + B\Omega^2\right)(A_g^{\,2} + A_t^{\,2} + A_+^{\,2} + A_-^{\,2})$$

$$- \frac{K}{2m}\,(x^2 + y^2)\ . \qquad (22)$$

We now define the following constants as:
the gradient sensing mode frequency

$$\omega_g^{\,2} = \frac{k'}{m} = \frac{k}{m} + B\Omega^2\ , \qquad (23)$$

the reduced mass of the sensor in the translational mode

$$\mu = \frac{M + 4m}{2m} , \tag{24}$$

and the mount translational frequency

$$\Omega_m = \frac{K}{M + 4m} . \tag{25}$$

Substituting into the Lagrangian and rearranging, we obtain

$$\begin{aligned} L = {} & \mu[\dot{x}^2 + \dot{y}^2 + 2\Omega(x\dot{y} - y\dot{x}) + (\Omega^2 - \Omega_m^2)(x^2 + y^2)] + \sqrt{2}(\dot{x} - \Omega y)(\dot{A}_+ - \Omega A_-) \\ & + \sqrt{2}(\dot{y} + \Omega x)(\dot{A}_- + \Omega A_+) + \frac{1}{2}\left(\frac{I + 4ma^2}{m}\right)\dot{\theta}^2 + 2a\dot{\theta}\dot{A}_t \\ & + \frac{1}{2}(\dot{A}_g^2 + \dot{A}_t^2 + \dot{A}_+^2 + \dot{A}_-^2) - \frac{1}{2}\omega_g^2(A_g^2 + A_t^2 + A_+^2 + A_-^2) \end{aligned} \tag{26}$$

The equation of motion for the gravity gradient sensing mode is given by

$$\frac{d}{dt}\frac{\partial L}{\partial \dot{A}_g} - \frac{\partial L}{\partial A_g} = 0 = \ddot{A}_g + \omega_g^2 A_g \tag{27}$$

which has the solution

$$A_g = A e^{i\omega_g t} \tag{28}$$

where the frequency of the resonant mode is given by the spring constant k and mass of the arms as modified by the centrifugal rotation

$$\omega_g^2 = \frac{k}{m} + B\Omega^2 \quad . \tag{29}$$

We note here that the frequency of this mode is not constant but shifts upward under rotation. This effect is borne out by the experimental results and is due to the increase in the effective spring constant from the centrifugal force acting on the sensor arms as gravity on a pendulum. However, the centrifugal force does not simulate gravity exactly since it is not a uniform field but extends radially outward. If the pivot point of the arm were at the center of rotation (b = 0), the frequency of the mode would be independent of the rotational speed, since the mass on the end of the arm would not see any variation in the centrifugal potential as the arm vibrated.

The equation of motion for the torsional mode is given by

$$\frac{d}{dt}\frac{\partial L}{\partial \dot{A}_t} - \frac{\partial L}{\partial A_t} = 0 = 2a\ddot{\theta} + \ddot{A}_t + \omega_g^2 A_t = 0 \tag{30}$$

where we eliminate the term containing the variation in sensor rotation speed $\ddot{\theta} = \ddot{\phi}$ by taking

$$\frac{d}{dt}\frac{\partial L}{\partial \dot{\theta}} - \frac{\partial L}{\partial \theta} = 0 = \left(\frac{I + 4ma^2}{m}\right)\ddot{\theta} + 2a\ddot{A}_t \tag{31}$$

or

$$\ddot{\theta} = -\frac{2ma}{I + 4ma^2}\ddot{A}_t \tag{32}$$

Substituting (32) into (30), we obtain

$$\left[1 - \left(\frac{4ma^2}{I + 4ma^2}\right)\right] \ddot{A}_t + \omega_g^2 A_t = 0 \quad . \tag{33}$$

When we solve this equation, we find that the natural frequency of the torsional mode is related to the gradient sensing mode frequency by

$$\omega_t^2 = \left(\frac{I + 4ma^2}{I}\right) \omega_g^2 \quad . \tag{34}$$

Here we note that the torsional mode frequency starts off higher than the gradient sensing mode frequency, provided the moment of inertia I of the central mass is not too large, and increases with rotation speed in the same manner. This behavior is borne out by the experimental results. An isolated sensor usually has a sufficiently small central mass that the torsional mode frequency is considerably higher than the gradient sensing mode frequency and rises with increasing rotation speed. However, if the sensor is firmly attached to a large sensor chamber, the torsional mode frequency shifts down toward the gradient sensing mode frequency.

The equations of motion for the four translational modes cannot be solved independently since they interact with each other. The four equations are

$$\frac{d}{dt}\frac{\partial L}{\partial \dot{x}} - \frac{\partial L}{\partial x} = 2\mu \left[\ddot{x} - 2\Omega \dot{y} - (\Omega^2 - \Omega_m^2)\, x\right]$$

$$+ \sqrt{2}\left[\ddot{A}_+ - 2\Omega A_- - \Omega^2 \dot{A}_+\right] = 0 \tag{35}$$

$$\frac{d}{dt}\frac{\partial L}{\partial \dot{y}} - \frac{\partial L}{\partial y} = 2\mu\left[\ddot{y} + 2\Omega\dot{x} - (\Omega^2 - \Omega_m{}^2)\, y\right]$$

$$+ \sqrt{2}\left[\ddot{A}_- + 2\Omega\dot{A}_+ - \Omega^2 A_-\right] = 0 \qquad (36)$$

$$\frac{d}{dt}\frac{\partial L}{\partial \dot{A}_+} - \frac{\partial L}{\partial A_+} = \sqrt{2}\left[\ddot{x} - 2\Omega\dot{y} - \Omega^2 x\right] + \ddot{A}_+ + \omega_g{}^2 A_+ = 0 \qquad (37)$$

$$\frac{d}{dt}\frac{\partial L}{\partial \dot{A}_-} - \frac{\partial L}{\partial A_-} = \sqrt{2}\left[\ddot{y} + 2\Omega\dot{x} - \Omega^2 y\right] + \ddot{A}_- + \omega_g{}^2 A_- = 0 \qquad (38)$$

We now define a right and left handed circularly polarized mode for the translational modes of the mount

$$R = \frac{1}{\sqrt{2}}(x + iy) \qquad (39)$$

$$L = \frac{1}{\sqrt{2}}(x - iy) \qquad (40)$$

along with the right and left handed modes for the sensor

$$A_r = \frac{1}{\sqrt{2}}(A_+ + iA_-) \qquad (41)$$

$$A_\ell = \frac{1}{\sqrt{2}}(A_+ - iA_-) \ . \qquad (42)$$

These can then be used to express eqs. (35) to (38) in an equivalent form

$$2\mu\left[\ddot{R} + 2i\Omega\dot{R} - (\Omega^2 - \Omega_m{}^2)\,R\right] + \sqrt{2}\left[\ddot{A}_r + 2i\Omega\dot{A}_r - \Omega^2 A_r\right] = 0 \qquad (43)$$

$$2\mu\left[\ddot{L} - 2i\Omega\dot{L} - (\Omega^2 - \Omega_m{}^2)\,L\right] + \sqrt{2}\left[\ddot{A}_\ell - 2i\Omega\dot{A}_\ell - \Omega^2 A_\ell\right] = 0 \qquad (44)$$

$$\ddot{A}_r + \omega_g{}^2 A_r + \sqrt{2}\left[\ddot{R} + 2i\Omega\dot{R} - \Omega^2 R\right] = 0 \qquad (45)$$

$$\ddot{A}_\ell + \omega_g{}^2 A_\ell + \sqrt{2}\left[\ddot{L} - 2i\Omega\dot{L} - \Omega^2 L\right] = 0 \qquad (46)$$

Notice that instead of all four mode amplitudes appearing in each equation indicating coupling between all four modes as they did in eqs. (35) to (38), we now find that the right handed circularly polarized mount mode interacts only with the right handed sensor mode and similarly for the two left handed modes.

The equations now only have to be solved in pairs, and the only difference between the two pairs of equations is the direction of rotation $\pm\Omega$.

Assuming solutions of the form

$$A_r = A e^{\pm i\omega t} \qquad (47)$$

$$R = R e^{\pm i\omega t} \qquad (48)$$

and using them in (43) and (45) we obtain a pair of equations

$$(\omega_g{}^2 - \omega^2)\,A - \sqrt{2}\left[\omega^2 \pm 2\omega\Omega + \Omega^2\right] R = 0 \qquad (49)$$

$$+2\mu\left[\omega^2 \pm 2\omega\Omega + \Omega^2 - \Omega_m{}^2\right] R + \sqrt{2}\,(\omega^2 \pm 2\omega\Omega + \Omega^2)\,A = 0 \qquad (50)$$

Rearranging (49)

$$A = \sqrt{2}\,\frac{(\omega \pm \Omega)^2}{(\omega_g{}^2 - \omega^2)}\,R \qquad (51)$$

and substituting it into (50), we obtain

$$2\mu\left[(\omega \pm \Omega)^2 - \Omega_m{}^2\right] R + 2\,\frac{(\omega \pm \Omega)^4}{(\omega_g{}^2 - \omega^2)}\,R = 0 \qquad (52)$$

or

$$(\omega \pm \Omega)^4 + \mu(\omega_g{}^2 - \omega^2)\left[(\omega \pm \Omega)^2 - \Omega_m{}^2\right] = 0 \qquad (53)$$

The four solutions to this fourth order equation in ω then tell us the vibrational frequencies of the four translational modes as a function of the rotation rate Ω, the mass ratio of the sensor masses $\mu = \frac{M + 4m}{2m}$, the basic mount frequency $\Omega_m{}^2 = \frac{K}{M + 4m}$, and the frequency of the gradient sensing mode ω_g. Since the gradient sensing mode frequency is also a function of rotation speed we can either express the dependence directly

$$(\omega \pm \Omega)^4 + \frac{M + 4m}{2m}\left(\frac{k}{m} + B\Omega^2 - \omega^2\right)\left[(\omega \pm \Omega)^2 - \frac{K}{M + 4m}\right] = 0 \qquad (53a)$$

or can normalize it out by taking the ratio of all the frequencies with respect to the gradient sensing mode frequency

$$\left(\frac{\omega}{\omega_g} \pm \frac{\Omega}{\omega_g}\right)^4 + \mu\left[1 - \frac{\omega^2}{\omega_g{}^2}\right]\left[\left(\frac{\omega}{\omega_g} \pm \frac{\Omega}{\omega_g}\right)^2 - \frac{\Omega_m{}^2}{\omega_g{}^2}\right] = 0\,. \qquad (53b)$$

In general it is necessary to use a computer to find the solutions to (53); however, under certain simplified conditions the equation reduces in order and can be solved.

EXAMINATION OF BEHAVIOR OF NORMAL MODE FREQUENCIES

In order to examine the behavior of the four translational mode frequencies, a series of plots of mode response frequencies ω as a function of rotation speed Ω was made for various values of the mount frequency Ω_m. These plots were all made using the normalized equation (53b).

The first plot (Fig. 4) shows the resonance behavior of a sensor on a very weak mount ($\Omega_m \approx 0$). For the case where the central mass of the sensor is negligible ($M \ll m$), the sensor translational modes start at $\omega_\pm = \sqrt{2}\ \omega_g$ and then split as the sensor starts rotating. When the rotation speed is at the desired operating point ($2\Omega = \omega_g$), the two sensor translational modes are at

$$\omega = \frac{1}{2}\left(\sqrt{10} \pm 1\right)\omega_g \tag{54}$$

or

$$\omega_+ = 2.081\ \omega_g \tag{55a}$$

$$M \ll m\ .$$

$$\omega_- = 1.081\ \omega_g \tag{55b}$$

If the mass of the central hub is increased so that $M = m$, the sensor translational mode starts out at $\omega_\pm = 1.29\ \omega_g$ and again splits under rotation in the same manner. At the desired operating speed the two frequencies are

$$\omega_+ = 1.728\ \omega_g \tag{56a}$$

$$M = m$$

$$\omega_- = 1.062\ \omega_g \tag{56b}$$

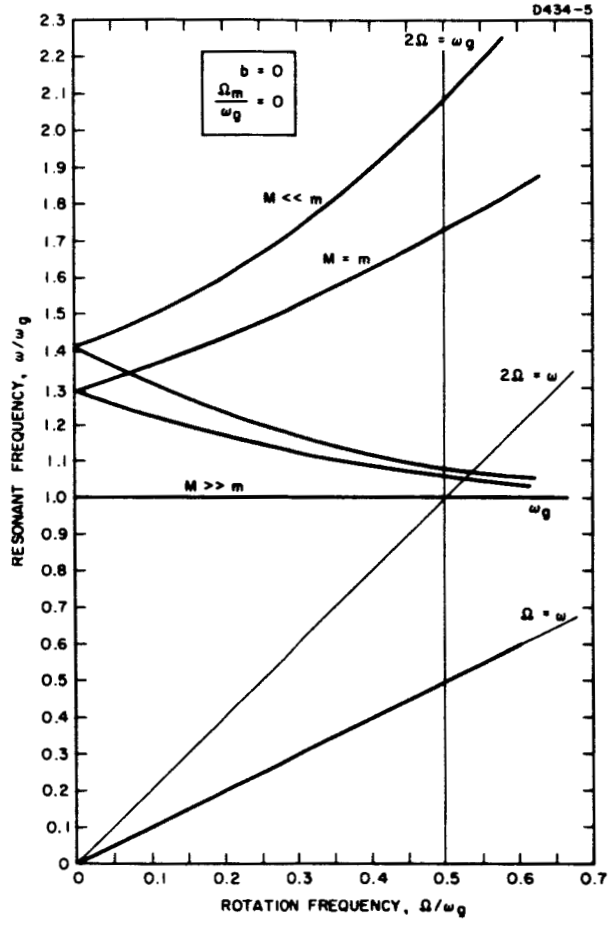

Fig. 4. Predicted translational mode splitting ($\Omega_m = 0$).

For a large central mass $M \gg m$, the sensor translational modes start out at

$$\omega_{\pm} = \omega_g \qquad M \gg m \tag{57}$$

and do not split under rotation.

From this set of curves we see that it is desirable to keep the central mass of the sensor as small as possible. In this manner we can obtain a higher degree of frequency separation between the gravity gradient sensing mode at ω_g and the vibration sensitive translational modes. As a practical matter it is difficult to make the central mass smaller than the arm masses, and in most of our sensors $M \approx m$. Because of this we assumed $M = m$ for the rest of our curves.

The next four graphs (Figs. 5 through 8) show the effect of increasing the frequency or stiffness of the mount. As the basic mount frequency is increased, the sensor translational modes are pushed upward away from the gravity gradient sensing mode, thus helping in the effort to maintain adequate frequency separation.

However, if the basic mount frequency is made higher, we find that when the mount resonance splits under rotation, the higher mode becomes very close to the gradient sensing mode at the desired operating speed ($\Omega = \frac{1}{2}\omega_g$).

Since our sensors are designed to be rotated at a rate which is half of the gradient sensing mode vibration frequency, we also calculated solutions to eq. (53b) assuming that $\Omega = \frac{1}{2}\omega_g$, but varying the mass ratio and the basic mount frequency Ω_m. These are plotted in Fig. 9. From these curves we see that changing the mass ratio does not aid appreciably in the problem of obtaining frequency separation, and that an optimum value for the basic mount frequency is around $\Omega_m = 0.5\,\omega_g$. From Figs. 6, 7, and 9, however, we see that for a mount at $\Omega_m = 0.5\,\omega_g$, the lower mount vibrational mode has a resonance at zero frequency for speeds of $\Omega = \frac{1}{2}\omega_g$, which is a possible point of instability. The best choice for a mount frequency would seem to be $\Omega_m = 0.55\,\omega_g$.

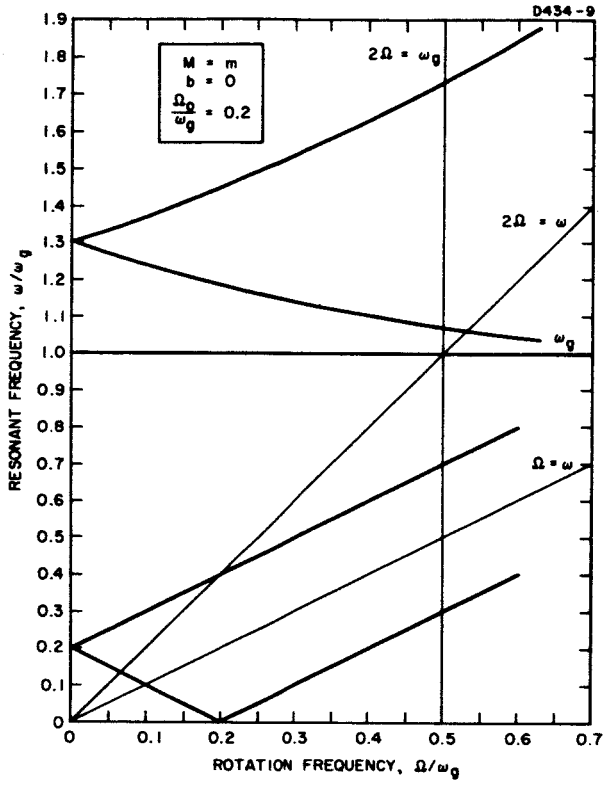

Fig. 5. Predicted translational mode splitting ($\Omega_m = 0.2\ \omega_g$).

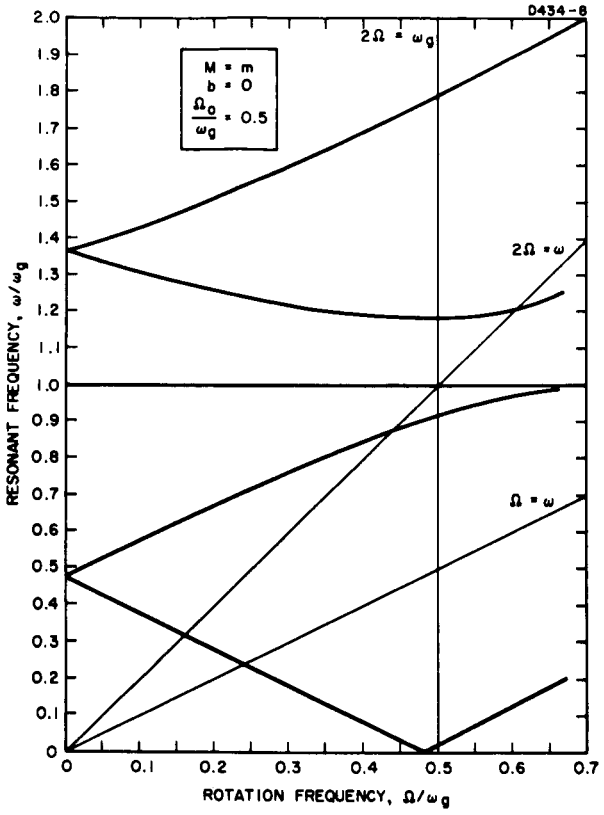

Fig. 6. Predicted translational mode splitting ($\Omega_m = 0.5\ \omega_g$).

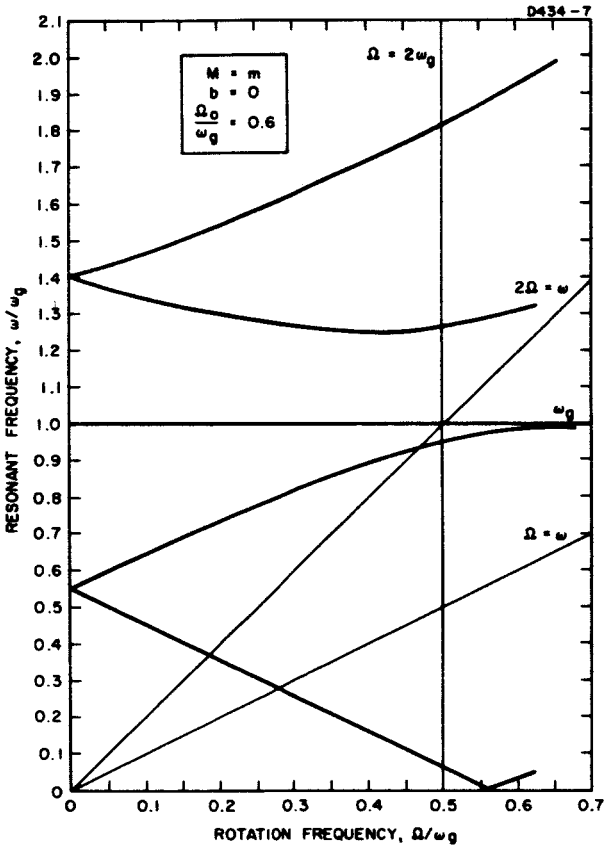

Fig. 7. Predicted translational mode splitting ($\Omega_m = 0.6\ \omega_g$).

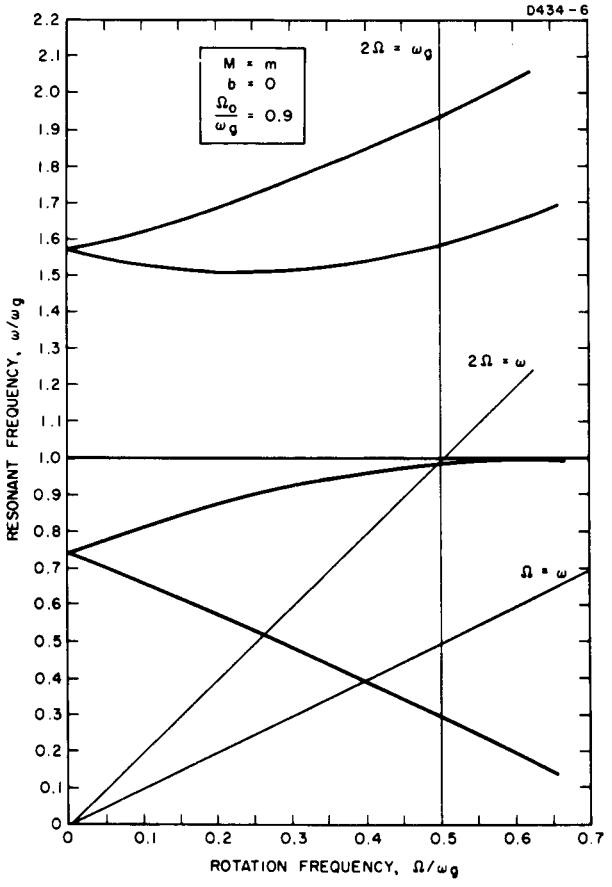

Fig. 8. Predicted translational mode splitting ($\Omega_m = 0.9\ \omega_g$).

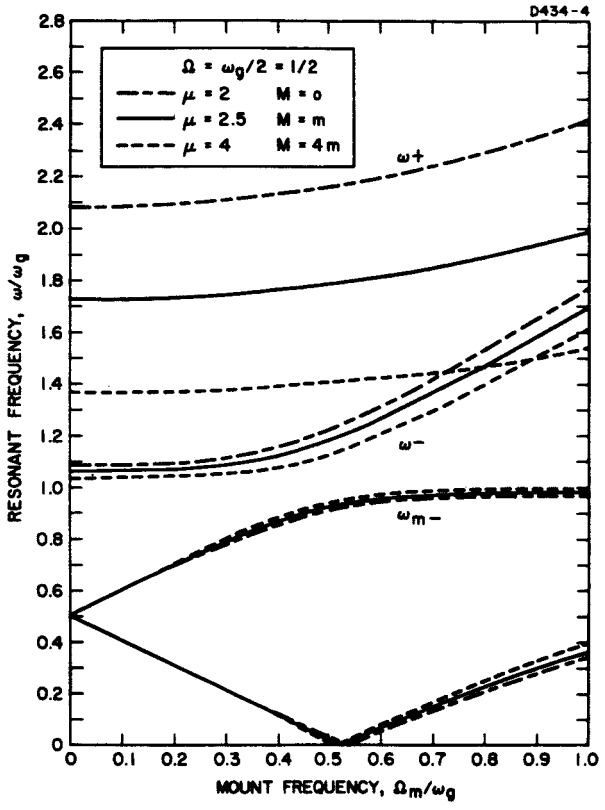

Fig. 9. Predicted translational mode splitting ($\Omega = 1/2\ \omega_g$).

The basic mount frequency is that which would be measured if the sensor arms were held fixed. The actual measured frequency is a little lower than this because of the interaction between the sensor modes and the mount modes.

COMPARISON OF THEORY AND EXPERIMENT

Data on sensor mode frequencies have been taken on various sensors during the experimental work on our program, and in general the theory agrees well with the data.

Sensor – Mount Interaction At $\Omega = 0$

If we assume that the sensor and mount are not rotating ($\Omega = 0$), then (53b) simplifies somewhat to become

$$\left(\frac{\omega}{\omega_g}\right)^4 + \mu\left[1 - \left(\frac{\omega}{\omega_g}\right)^2\right]\left[\frac{\omega^2}{\omega_g^2} - \frac{\Omega_m^2}{\omega_g^2}\right] = 0 . \qquad (58)$$

When this is plotted for $\mu = 3.07$ ($M = 2.15m$) we obtain the curves shown in Fig. 10. The light lines $\omega_\pm$ and Ω_m indicate what the sensor translational modes and the mount translational modes would do if they did not interact with each other.

One of our sensors had been tested with a large number of possible mounts (see Fig. 11). The frequency data from these tests were normalized and are plotted as the points in Fig. 10. The agreement of the theory with the experiment is excellent. This curve can be used to determine the basic mount frequency when the three resonant frequencies of the interacting system are known, and will aid in the optimum mount design.

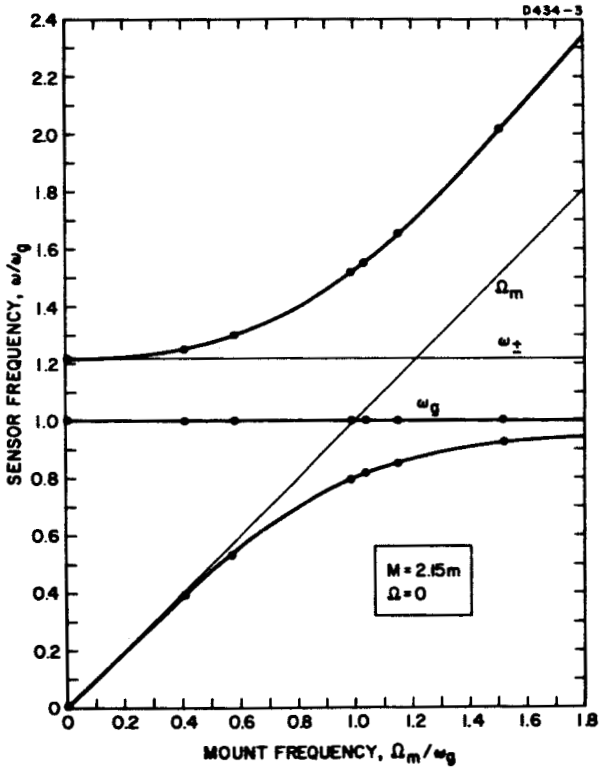

Fig. 10. Mount-sensor interaction (nonrotating).

Rotating Sensor on Soft Mount

A very nice set of sensor resonant frequency data had been taken on a rotating cruciform hanging from a rubber band (see Fig. 12). The rubber band had a very low natural frequency, and therefore $\Omega_m = 0$. There was an instability at low rotation rates, but after this was passed through and the sensor rotated above the resonance point, it was very stable. The data are plotted in Fig. 13. Four points from the data (large points) were then used to determine the four sensor parameters $\frac{k}{m}$, B, $\frac{I + 4ma^2}{I}$ and, $\mu = \frac{M + 4m}{2m}$.

These parameters were then used in the three equations

$$\omega_g^2 = \frac{k}{m} + B\Omega^2 \tag{59}$$

$$\omega_t^2 = \left(\frac{I + 4ma^2}{I}\right)\left(\frac{k}{m} + B\Omega^2\right) \tag{60}$$

$$(\omega_\pm \pm \Omega)^2 + \mu\left(\frac{k}{m} + B\Omega^2 - \omega_\pm^2\right) = 0 \tag{61}$$

to obtain the theoretical curves. The agreement with the data is excellent. The highest set of data seems to be the upper half of a split torsional mode. It is believed to result from the effect of the moment of inertia of the arm masses which was neglected in the theoretical calculations.

Rotating Sensor on Hard Mount

Only one set of frequency data is available for a rotating sensor on a fairly rigid mount. The mounting structure used was a wire attached to the sensor at the center and held at the ends by the lid and base of a sensor vacuum chamber (see Fig. 14). The data are shown in Fig. 15. The two translational modes of the sensor and the two translational modes of the mount were not the same at zero rotation speed.

M4612

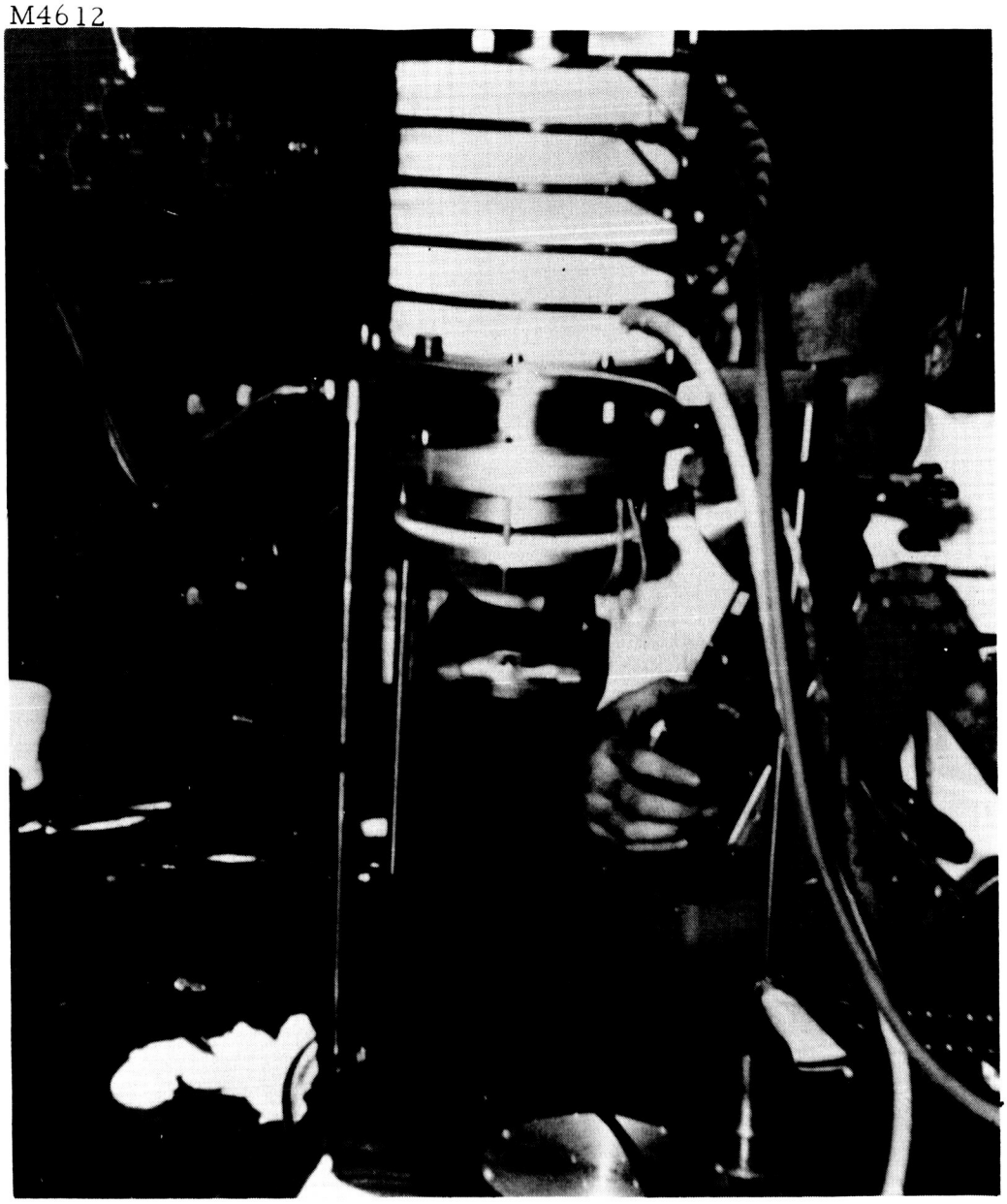

Fig. 12. Sensor rotating on rubber band suspension under magnetic bearing.

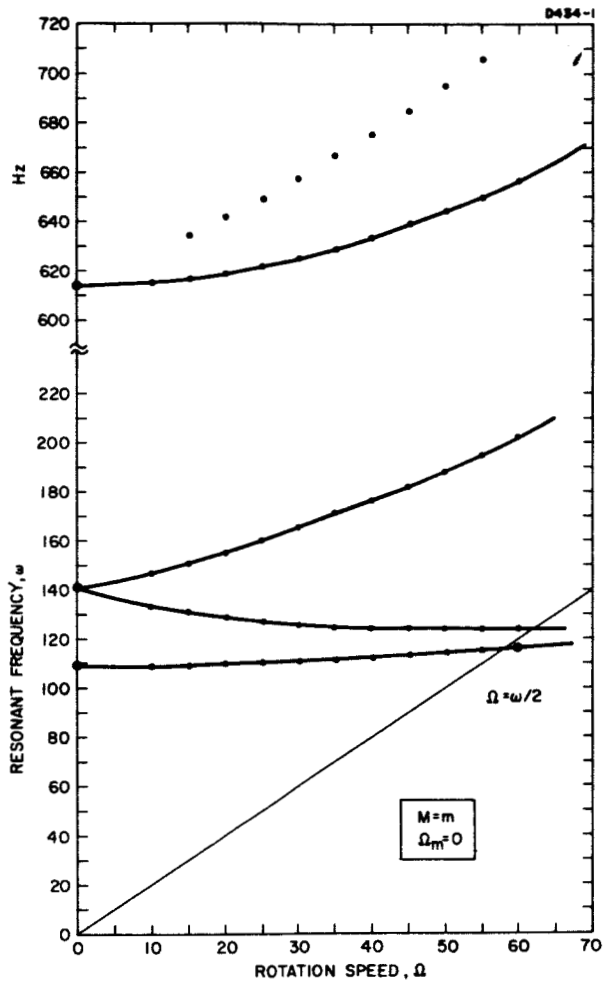

Fig. 13. Rotating sensor system resonant modes on soft mount.

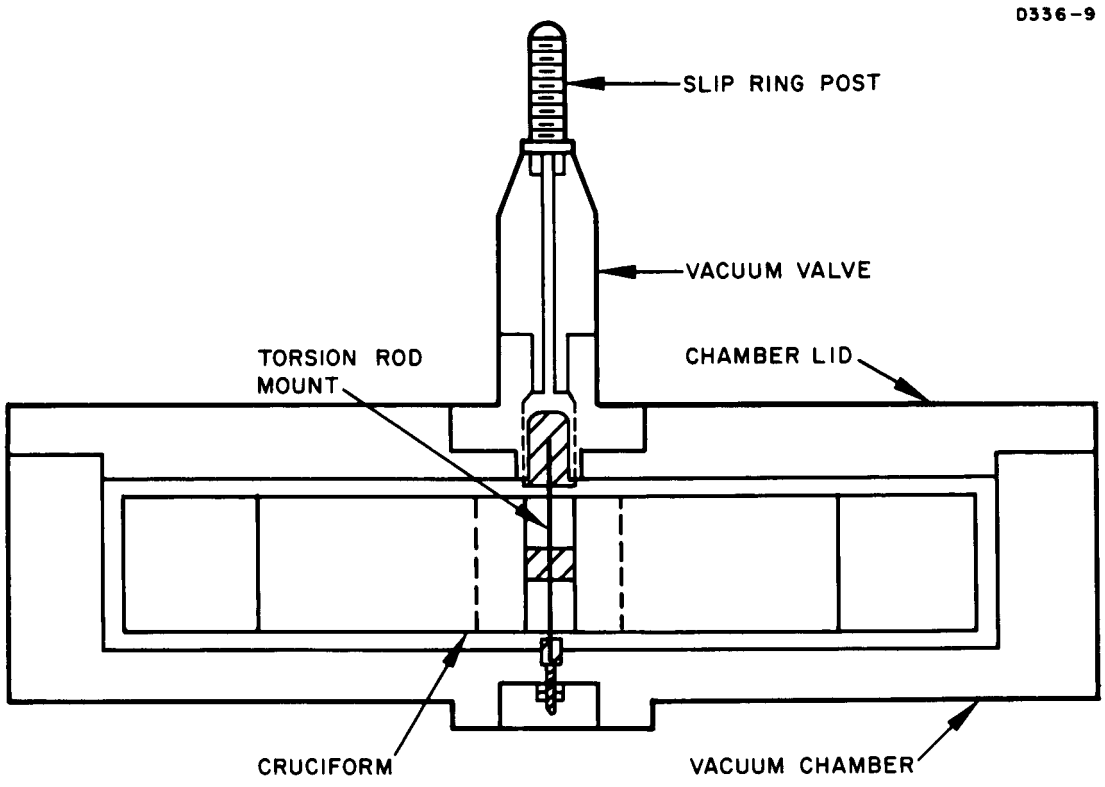

Fig. 14. Cruciform sensor on torsion wire mount.

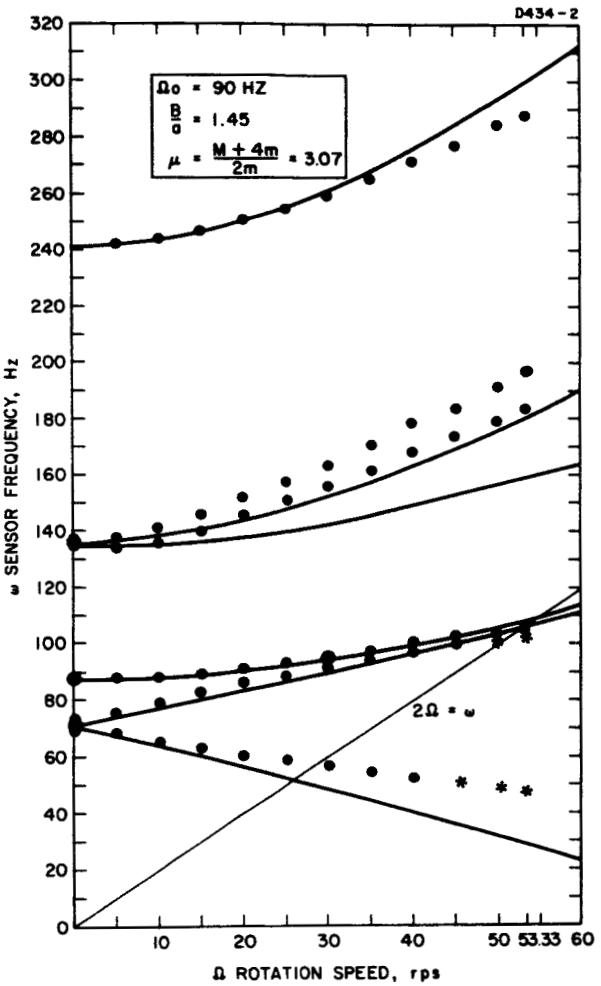

Fig. 15. Rotating sensor resonant modes on hard mount.

This indicates that the sensor had a considerable asymmetry in construction.

This time five points were taken in order to determine the sensor parameters and the mount frequency. These parameters were then used in (59), (60), and (53) to obtain the theoretical curves.

Although the theoretical curves have the same general behavior as the actual measured data, the fit is nowhere near as good as in Fig. 10 and 13. It is believed that this results primarily because the torsion wire is not a linear spring, but its spring constant depends upon the tension in the wire and the tension was increasing during rotation because of the centrifugal force acting on the unbalance in the sensor.

CONCLUSIONS

We have developed a mathematical model of a rotating, spring mounted, cruciform gravitational gradient sensor and have obtained equations describing the behavior of the normal mode frequencies of the system as a function of the system parameters and the rotation speed. These equations agree well with the data from actual sensors and can be used to aid in the design of optimum mount-sensor structures. The theory and experiment indicate that it is possible to operate a sensor at the desired rotation speed of one-half of the gradient sensing mode frequency and still maintain adequate frequency separation between the vibration sensitive translational modes and the gradient sensing mode.

REFERENCES

1. R. L. Forward, "Rotating tensor sensors," Bull. Am. Phys. Soc. 9, 711 (1964).

2. R. L. Forward, "Gravitational Mass Sensor," Proc. Symp. on Unconventional Inertial Sensors (Farmingdale, N. Y., 1963), pp. 36-60.

3. J. C. Crowley, S. S. Kolodkin, and A. M. Schneider, "Some properties of the gravitational field and their possible application to space navigation," IRE Trans. SET-4, 47-54 (1959).

4. M. Streicher, R. Zehr, and R. Arthur, "An Inertial Guidance Technique Usable in Free Fall," Proc. Nat. Aero. Elec. Conf. (Dayton, Ohio, 1959), pp. 768-772.

5. J. J. Carroll and P. M. Savet, "Space navigation and exploration by gravity difference detection," IAS Paper 59-61, IAS National Summer Meeting, Los Angeles, 1959; also Aerospace Eng. 18, 44-47 (1959).

6. R. E. Roberson, "Methods for the Control of Satellites and Space Vehicles, Vol. 1, Sensing and Actuating Mechanisms," WADD Tech. Rpt. 60-643 (1960).

7. R. E. Roberson, "Gravity gradient determination of the vertical," ARS J. 31, 1509-1515 (1961).

8. P. Savet, "Attitude control of orbiting satellites at high eccentricity," ARS J. 32, 1577-1582 (1962).

9. J. W. Diesel, "A new approach to gravitational gradient determination of the vertical," AIAA J. 2, 1189-1196 (1964).

10. R. E. Roberson, "Establishment of the Center of Mass and Rotational State of a Space Vehicle by Inertial Techniques," Proc. XV Inter. Astro. Cong., Warsaw, 1964 (to be published).

11. R. L. Forward, "Rotating Gravitational and Inertial Sensors," presented at the AIAA Unmanned Spacecraft Meeting, Los Angeles, 1-4 March 1965.

12. C. C. Bell, R. L. Forward and J. R. Morris, "Mass Detection by Means of Measuring Gravity Gradients," presented at AIAA Second Annual Meeting, San Francisco, Calif., 26-29 July 1965.

13. R. L. Forward, D. M. Zipoy, and J. Weber, "Measurement of dynamic gravitational fields," Bull. APS 7, 320 (1962).